

ESD ACCESSION LIST

TRI Call No. 75572
Copy No. 1 of 1 cys.

ESD RECORD COPY

RETURN TO
SCIENTIFIC & TECHNICAL INFORMATION DIVISION
(TRI), Building 1210

TRI FILE COPY

Technical Report

487

Multiple-Pulse
Monopulse Accuracy

D. H. Pruslin

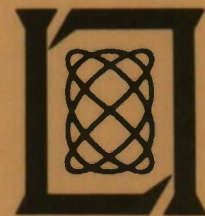
19 November 1971

Prepared under Electronic Systems Division Contract F19628-70-C-0230 by

Lincoln Laboratory

MASSACHUSETTS INSTITUTE OF TECHNOLOGY

Lexington, Massachusetts



AD0737369

Approved for public release; distribution unlimited.

MASSACHUSETTS INSTITUTE OF TECHNOLOGY
LINCOLN LABORATORY

MULTIPLE-PULSE MONOPULSE ACCURACY

D. H. PRUSLIN

Group 96

TECHNICAL REPORT 487

19 NOVEMBER 1971

Approved for public release; distribution unlimited.

LEXINGTON

MASSACHUSETTS

The work reported in this document was performed at Lincoln Laboratory, a center for research operated by Massachusetts Institute of Technology, with the support of the Department of the Air Force under Contract F19628-70-C-0230.

This report may be reproduced to satisfy needs of U.S. Government agencies.

Non-Lincoln Recipients

PLEASE DO NOT RETURN

Permission is given to destroy this document
when it is no longer needed.

ABSTRACT

This report presents results from a simulation of an amplitude comparison monopulse system employing pulse integration (multiple pulses). Maximum-likelihood-angle estimators and approximations to them are derived. The accuracies (precision and bias) of these estimators are obtained by computer simulation for coherent and incoherent processing, and targets located on- and off-boresight. Results are presented as functions of signal-to-noise ratio and number of pulses integrated. The effects of imperfect knowledge of target doppler, phase, and amplitude are included. Theoretical bounds on the precision of the estimators are derived and compared with the simulation results.

Accepted for the Air Force
Joseph R. Waterman, Lt. Col., USAF
Chief, Lincoln Laboratory Project Office

CONTENTS

| | |
|--|-----|
| Abstract | iii |
| I. INTRODUCTION | 1 |
| II. MONOPULSE ANGLE ESTIMATORS | 2 |
| III. INCOHERENT PROCESSING | 5 |
| A. Approximate Estimator | 5 |
| B. Maximum-Likelihood Estimator | 13 |
| C. Theoretical Bounds on Precision | 15 |
| IV. COHERENT PROCESSING | 17 |
| A. Approximate Estimator | 17 |
| B. Maximum-Likelihood Estimator | 22 |
| C. Theoretical Bounds on Precision | 22 |
| APPENDIX A - Monopulse Angle Estimators | 23 |
| APPENDIX B - Theoretical Bounds to Estimator Precision | 27 |

MULTIPLE-PULSE MONOPULSE ACCURACY

I. INTRODUCTION

One of the basic radar functions is angle measurement which, in its grossest form, is accomplished by radiating and receiving through a directive beam. If a target is detected, its spatial direction is taken to be the direction in which the beam is pointing. Because the beam pattern is relatively flat over some suitably defined beamwidth, the angle measurement precision is on the order of one beamwidth. That is, all one can really say is that the target is somewhere within the angular extent of the beam.

To improve this situation, a technique referred to as beam-splitting is commonly employed. The essence of this technique is to employ two beams. One beam pattern is still relatively flat over an angular extent corresponding to the basic antenna directivity. The second beam has a pattern which is relatively linear in angle over the extent of the first beam. Targets are detected in the flat beam and their spatial angles are measured by noting the relative amplitude of the signal in the linear beam and the flat beam. To the extent that the flat beam is really flat, and that the variation of the linear-beam pattern with angle is known, this technique appears to refine the precision of the angle measurement to well below a beamwidth. Among the basic limits to this precision are:

- (a) Uncertainties in the shapes of the set of beams.
- (b) Unknown offsets between the true and intended pointing directions of the beams.
- (c) Random noise additive to the received signals.

(In addition, contributions may include target glint or phase center motion, amplitude fluctuations which at least cause the signal-to-noise ratio (SNR) to vary, etc.)

The results reported below pertain to the precision limit imposed by random noise and, more specifically, to the effects on this precision of combining the data from a sequence of radar transmissions. At the verbal level, a number of questions come to mind. How should the amplitudes and phases of the beam signals on a single transmission be combined? How do the precision and accuracy of the angle estimate depend on SNR? How should the amplitudes and phases from multiple transmissions be combined? What is meant by "incoherent" and "coherent" processing in this context? How do the precision and accuracy vary with the number of pulses "integrated"? In the sections that follow, we will describe an analysis which provides a basis for answering these questions, and will present computer simulation (Monte Carlo) results based on this analysis.

Before turning to these results, we will make more explicit what they do not pertain to (refer to Fig. 1). "Angle estimation" denotes the process by which signals in the set of beams from N radar pulses are combined to produce an estimate of the angular location of a target. The target is assumed to be stationary in space over the time required to collect the N pulses. "Angle tracking" denotes a process in which a sequence of angle estimates is processed or filtered (either by analog or digital means, or both), resulting in a "steering command" which

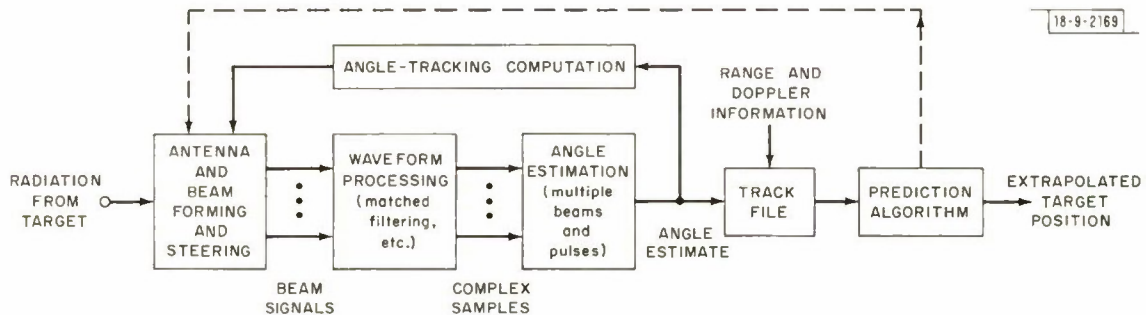


Fig. 1. Functions involving angle measurement.

moves the antenna beam with the goal of following target motion and thus not "breaking track" or losing the target. "Track prediction" denotes a process in which a sequence of angle estimates is combined with range and possibly range-rate measurements, and with a model of target dynamics, to produce an extrapolation of target position at another time. The track-prediction algorithm may also serve as the angle-tracking algorithm by producing "short-term" extrapolations for "immediate" use in steering the beam, or the angle-tracking algorithm may be distinct, perhaps simpler and using less data and, in the case of a dish, using analog processing.

In these terms, our results do not pertain to track prediction and, except for a few words, do not pertain to angle tracking. They pertain to the effects of additive random noise on angle estimation.

II. MONOPULSE ANGLE ESTIMATORS

This section describes a set of angle estimators whose statistical properties (mean and variance) will be demonstrated using simulation results appearing in the following sections. A comprehensive description of these estimators is presented in Appendix A.

The basis for our results is found in a paper by Hofstetter,¹ wherein he solves (as a sub-problem) the following problem. Consider a set of beams in which a target return may be present. N radar pulses are to be processed. The target, if present, is assumed to be fixed in space during the time required to transmit and receive the set of pulses. Its amplitude is unknown but constant (see Sec. III-A-4-d), and its doppler frequency is assumed known (see Sec. IV-A-3-b). On a given pulse, the carrier phase of the return signal is unknown but the same in all the beams. (We are assuming an amplitude-comparison monopulse system, implying a design in which there is no dependence of signal time-of-arrival on spatial angle in any beam. Thus, the value of the phase does not depend on the true target spatial angle or on which beam is examined. The phase may be thought of as depending on the fine range position of the target.) Over a set of pulses, two cases (incoherent and coherent) are considered for the phases. In the incoherent case, no relation between the phases on any two pulses is assumed (see Sec. III).

In the coherent case, the phase angle is unknown but assumed constant over the set of pulses (see Sec. IV, particularly IV-A-3). Added to the received signals is random noise, assumed independent from beam-to-beam, independent from pulse-to-pulse, Gaussian, and having zero mean and known variance.

Given this set of assumptions, Hofstetter derives the "generalized likelihood ratio" detection function and parameter estimates. In the present case, the receiver is assumed to compute the likelihood ratio (the ratio of the probability of seeing the observed data given that a target is present divided by this probability given that noise alone is present) with the unknown target attributes of amplitude, carrier phase, and spatial angle as parameters. The receiver then maximizes the likelihood ratio with respect to the unknown parameters, and compares the maximum with a threshold. If the threshold is exceeded, a target is considered present, and its parameters (in particular, its spatial angle) are taken to be those values which maximized the likelihood ratio.

For the special case of two beams (one beam constant-vs-angle and the other linear in angle), each a function of the same single spatial angle θ , the angle estimates for the incoherent and coherent cases are: $\hat{\theta}$ = the value of θ producing the maximum

$$\max_{\theta} \frac{\left[\sum_{k=1}^N [|y_{2k}|^2 + \theta^2 |y_{1k}|^2 + 2\theta |y_{1k}| |y_{2k}| \cos(\varphi_{2k} - \varphi_{1k})]^{1/2} \right]^2}{1 + \theta^2} \text{ incoherent} \quad (1)$$

and

$$\max_{\theta} \frac{\left| \sum_{k=1}^N [y_{2k} + \theta y_{1k}] \right|^2}{1 + \theta^2} \text{ coherent} \quad (2)$$

respectively.

In these expressions, y_{1k} denotes the complex amplitude of the received signal on the k^{th} pulse (target plus noise) at the output of a matched filter in the linear or difference channel, $|y_{1k}|$ and φ_{1k} being its amplitude and phase angle, respectively. The complex amplitude in the constant or sum channel is denoted by y_{2k} .

In addition to these estimators, a pair of approximate estimators are derived which take the form

$$\hat{\theta} = \frac{\sum_{k=1}^N |y_{1k}| \cos(\varphi_{1k} - \varphi_{2k})}{\sum_{k=1}^N |y_{2k}|} \text{ incoherent} \quad (3)$$

and

$$\hat{\theta} = \frac{\sum_{k=1}^N |y_{1k}| \cos(\varphi_{1k} - \hat{\psi})}{\left| \sum_{k=1}^N y_{2k} \right|}, \quad \hat{\psi} = \arg \left[\sum_{k=1}^N y_{2k} \right] \text{ coherent} \quad (4)$$

Note that in the coherent estimators [Eqs. (2) and (4)], the assumed constancy of phase angle between pulses is evidenced by vectorial addition of the beam signals from different pulses. In

the incoherent estimators [Eqs. (1) and (3)], it can be seen that no relation between the phase angles on different pulses is assumed, although the phase angles are still used on a pulse-by-pulse basis.

Prior to comparing the performance of the exact and approximate estimators, the most obvious difference between them is that the exact estimators require a search over the angle Θ , while the approximate estimators do not. That is, the approximate estimators evaluate a single function of the received data and produce an estimate. The exact estimators must evaluate a function of the received data for a number of values of the parameter Θ to produce an estimate. In practice, the granularity of the search over a discrete set of Θ values should be no larger than, and preferably smaller than, the inherent precision of the estimator. Otherwise, the resultant precision will be dominated by quantization error. The search requirement does not imply any innate difference in the maximization problem between the exact and approximate cases. It is a practical matter dictated by the inability to solve Eqs. (1) or (2) in closed form.

Ideally, one would like to determine the probability density functions for these estimates, as a function of true target angle Θ , SNR, and number of pulses integrated. In practice, it is not even feasible to obtain by analysis their means and variances. We have therefore obtained these quantities by simulation, and present the results below graphically. The basic format is a log-log plot whose vertical axis is standard deviation (and sometimes bias) of the estimator in normalized units. The horizontal axis is number of pulses integrated, increasing to the left due to the vagaries of graph paper. Each plot contains a family of curves parameterized on SNR. The direction of good estimator performance is down on the graph, i.e., in the direction of small standard deviation and bias. The normalized angle unit on the vertical axis should be interpreted as fractions of a beamwidth. To make this more specific, refer to Fig. 2. The sum beam is flat and of unit amplitude. The difference beam is linear and crosses unity amplitude

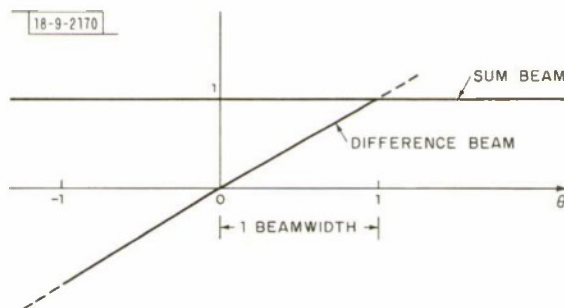


Fig. 2. Beam patterns.

at one unit of angle (ordinarily taken as the effective limit of operation). In fact, Eqs. (1) through (4) have been written with this convention implicit. The single-sided beamwidth is taken to be the point where the sum- and difference-beam amplitudes are equal, i.e., one angular unit. With this definition of beamwidth, the vertical axis on the plots is strictly measured in fractions of a beamwidth. Thus, if the beamwidth is half a degree, and the standard deviation of the estimate is 0.1 normalized unit, the standard deviation in degrees is 0.05.

The SNR referred to as E/N_0 on the plots is equal to the ratio of the voltage due to signal squared divided by the variance of the noise, both measured at the matched-filter output in the sum channel at the sampling time corresponding to a target centered in range. The variance is that of the RF (or IF) noise or either of its quadrature components, which is half the variance of the complex noise envelope.

III. INCOHERENT PROCESSING

A. Approximate Estimator

1. On-Boresight Results

a. Basic Performance

The basic performance of the approximate incoherent estimator with a true target angle of zero is shown in Fig. 3. We note that

- (1) The estimate is unbiased.
- (2) As the number of pulses N and the per-pulse SNR E/N_0 are increased, the standard deviation is asymptotic to

$$\sigma_{\theta} = \frac{1}{\sqrt{N} \sqrt{E/N_0}} \quad (5)$$

- (3) The precision therefore approaches a value corresponding to averaging N single-pulse estimates.

b. Effect of Using Phase for Sense Only

The term $\cos(\varphi_{1k} - \varphi_{2k})$ in Eq. (3) has two functions. Primarily, it provides sense information, i.e., on which side of boresight the target is located. One can see that when the noise is small the phase angles φ_{1k} and φ_{2k} are determined primarily by the target component of the beam signals, and will therefore be close to 0 or π depending on which side of boresight the target is located. Secondly, the term provides amplitude weighting. To see the effect of this weighting, the term $\cos(\varphi_{1k} - \varphi_{2k})$ can be replaced by $\text{sgn}[\cos(\varphi_{1k} - \varphi_{2k})]$, preserving the sense information and removing the amplitude weighting. Figure 4 shows the result of this change. We note that:

- (1) The estimate is still unbiased.
- (2) The precision is degraded quite uniformly over the whole plot by a factor of about 1.4.

c. Expurgated Estimate

In the results presented above, no attempt was made to discard estimates that were obviously dominated by noise, that is, occurrences when the estimate fell outside the monopulse range of $-1 \leq \theta \leq 1$. This accounts for the precision at 1 pulse and low E/N_0 being worse than a beamwidth. In Sec. d which follows, we will present results on the effects of amplitude fading, where there would be a greater tendency toward very "anomalous" estimates because of the probability of very low target amplitudes. To make a better comparison, we show in Fig. 5 how the results of Fig. 3 change when we discard all estimates which fall outside the range ± 1 . Related results are shown in Fig. 6 where we plot the probability of anomaly vs E/N_0 for the single-pulse estimator. We note that:

- (1) There is essentially no change for $E/N_0 \geq 10$ dB.
- (2) For $E/N_0 = 0$ dB, there is a change at 10 pulses or less, with the precision being improved to values below one beamwidth.
- (3) Correspondingly, the probability of getting an anomalous estimate decreases from about one in five at 0 dB to the order of 1 percent at 10 dB, for the single-pulse estimator. Essentially, no anomalies occur at 10 pulses or more, down to E/N_0 of 0 dB.

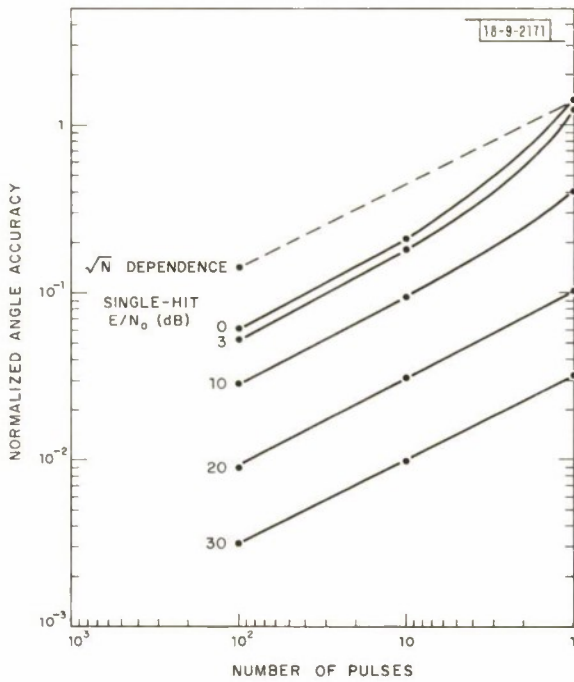


Fig. 3. Incoherent integration, target on monopulse boresight.

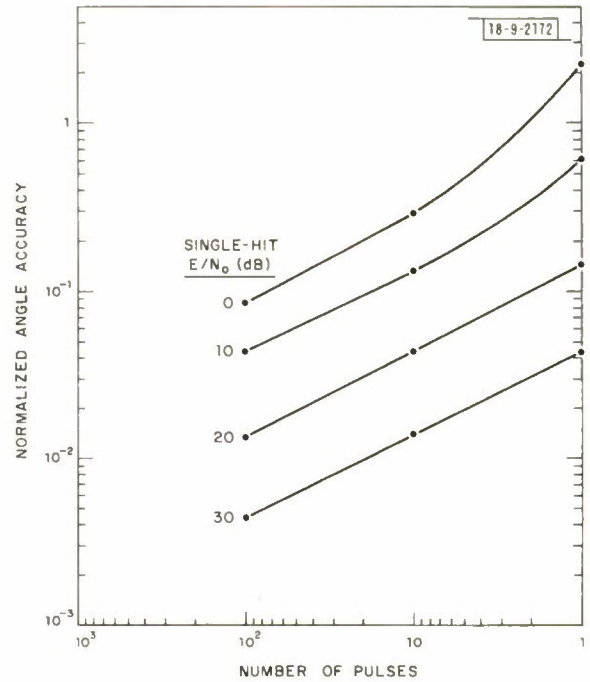


Fig. 4. Incoherent integration, phase used for sense only, target on monopulse boresight.

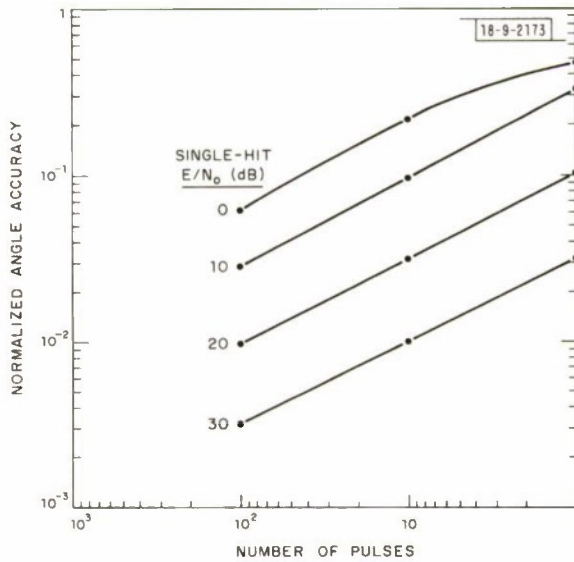


Fig. 5. Incoherent integration - on-boresight, expurgated at ± 1 beamwidth.

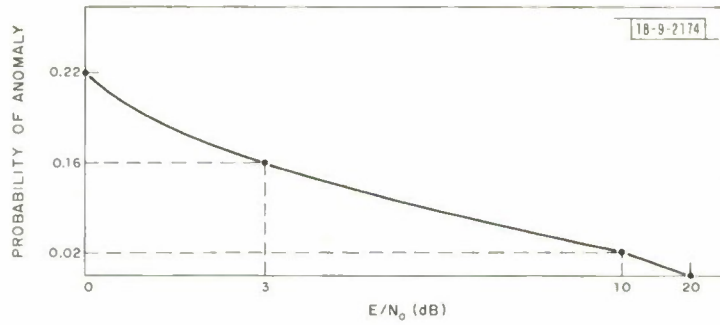


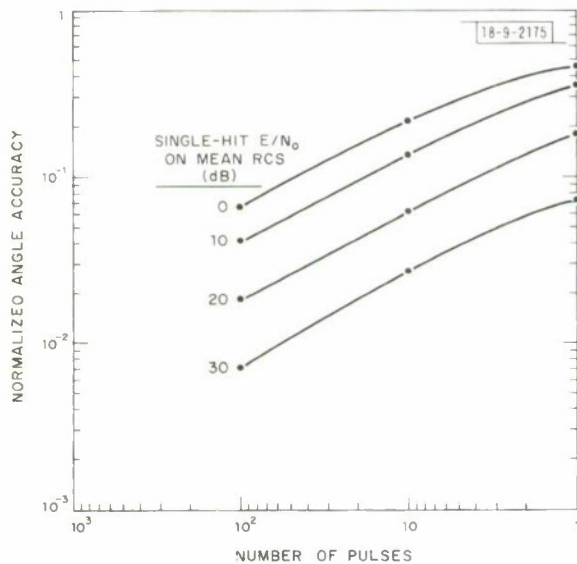
Fig. 6. Probability of anomaly for expurgated single-pulse estimator and nonfluctuating target.

d. Expurgated Estimate in the Presence of Amplitude Fading

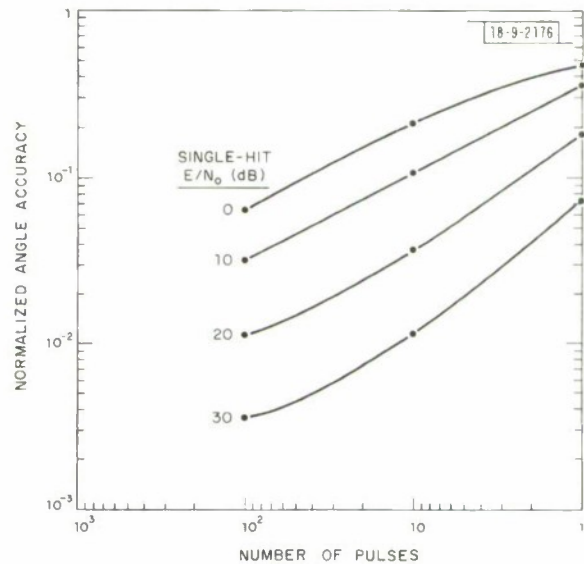
To explore the effect of violating the assumption that the target amplitude is constant, we computed the performance of the expurgated estimator on-boresight for a target whose cross section varies with an exponential probability density. If the cross section is represented by x , and has mean value \bar{x} , then the density function is

$$p(x) = \frac{1}{\bar{x}} e^{-(x/\bar{x})} \quad (6)$$

Figure 7(a) shows the results for a scan-to-scan fade (Swerling I) in which the cross section is random but remains constant over the set of N pulses used to make the estimate. Figure 7(b) shows the corresponding results for a pulse-to-pulse fade (Swerling II) in which the cross section is random and takes on an independent value on each pulse. The corresponding probability of



(a) Scan-to-scan fade with exponential RCS density (Swerling I).



(b) Pulse-to-pulse fade with exponential RCS density (Swerling II).

Fig. 7(a-b). Incoherent integration - on-boresight, angle estimate expurgated at ± 1 beamwidth.

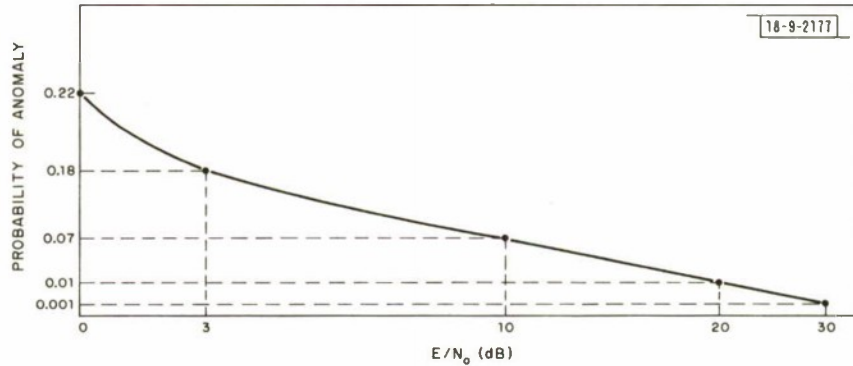


Fig. 8. Probability of anomaly for expurgated single-pulse estimator and fluctuating target.

anomaly for the single-pulse estimate, which is of course the same for the scan-to-scan and pulse-to-pulse fades, is shown in Fig. 8. In Figs. 7(a) and (b), E/N_0 represents the single-hit SNR on the mean cross section. For the exponential density function, the median or 50-percent point is 0.69 times the mean. Thus, E/N_0 on the median is 1.6 dB less than on the mean. We note that:

- (1) For the scan-to-scan fade, even with the anomalous estimates removed by expurgation, it is the low cross-section probability of the fade that dominates, not the high cross-section probability. This is evidenced by the fact that at 0-dB E/N_0 , there is no difference between Figs. 5 and 7(a), so that the probability of high cross section is not helping, while at 30 dB the precision with fading is worse than without fading, by a factor between 2 and 3, so that the probability of low cross section has a degrading effect.
- (2) The pulse-to-pulse fade is less detrimental to the precision of the estimate. While the increase in degradation factor (relative to no fading) with E/N_0 is, of course, the same as for the scan-to-scan fade at one pulse integrated, the degradation decreases with the number of pulses integrated, and is small beyond 10 pulses. The pulse-to-pulse fade apparently reduces the effectiveness of small cross-section hits in producing bad estimates.
- (3) The increased probability of seeing a low cross section relative to the nonfading target manifests itself in a slower decrease of probability of anomaly with E/N_0 for the single-pulse estimator. At 10 dB, this probability is on the order of a percent for the fixed target. It is between 4 and 5 times higher for the fading target at this point, and another 10 dB of SNR is required to reduce it to 1 percent. As with the fixed target, there is essentially no probability of anomaly if 10 or more pulses are integrated.
- (4) With the scan-to-scan fade, the improvement in precision between 1 and 100 pulses is such that it would be slightly better to average 100 individual single-pulse estimates at E/N_0 of 10 dB or less, while there would be no difference at 20 dB or more (averaging individual estimates reduces the standard deviation as $1/\sqrt{N}$).

With the pulse-to-pulse fade, averaging individual single-pulse estimates would be slightly superior at an E/N_0 of 0 dB, and progressively inferior as E/N_0 increased from 10 dB upward.

In either case, a cost involved in averaging single-pulse estimates is that the probability of anomaly is essentially zero when 10 or more pulses are integrated, while it is nonzero for single-pulse estimates. It would therefore require somewhat more than 100 hits to produce 100 expurgated single-pulse estimates.

2. Off-Boresight Results

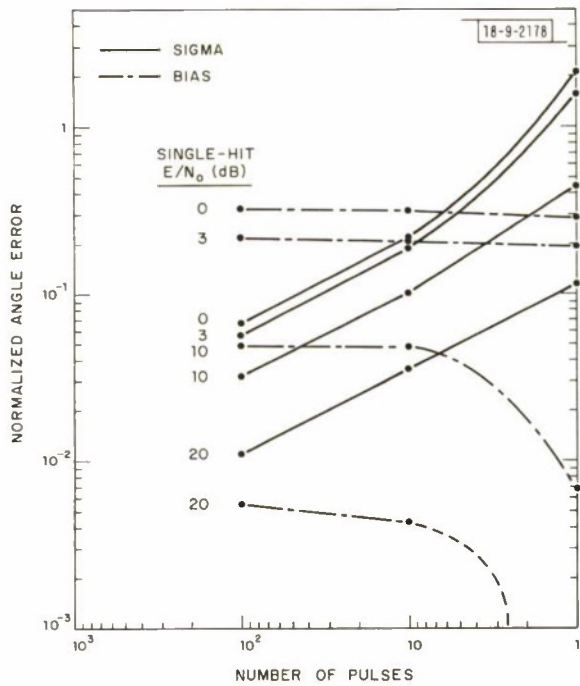
a. Basic Performance

When the true target angle θ is moved off the monopulse boresight (i.e., the direction in which the center of the set of beams is pointed), the behavior of the approximate estimator becomes more complicated. Figure 9(a) shows the performance when the target is halfway between the boresight and the edge of the beam ($\theta = 0.5$), while Fig. 9(b) shows the corresponding results for the target at the edge of the beam ($\theta = 1$). We note that:

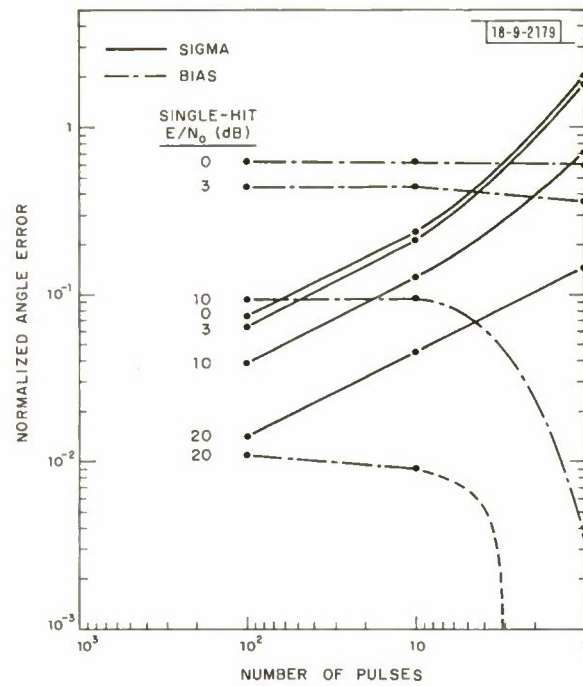
- (1) The estimate is biased, and the bias is directed toward boresight. That is, if the true target angle is a positive value, the mean value of the estimate is a smaller positive value; if the true angle is negative, the mean value of the estimate is negative and of smaller magnitude.
- (2) For a given target angle and number of pulses integrated, the magnitude of the bias (both absolute and relative to the standard deviation) increases with decreasing E/N_0 .
- (3) For a given target angle, the bias is essentially constant between 1 and 100 pulses at low E/N_0 (0 and 3 dB). At 10 dB or more, the bias builds up from a low value at one pulse to a higher value at 10 pulses and remains essentially constant out to 100 pulses.
- (4) Consequently, if one is starting from a fairly good SNR (10 dB or more), averaging a number of single-hit estimates may be preferable to forming one multiple-pulse estimate. For example, if E/N_0 is 10 dB and 100 pulses are processed with the target near the edge of the beam, a 100-pulse estimate would have precision ≈ 0.04 and bias ≈ 0.1 . By comparison, the average of 100 single-pulse estimates would have precision $\approx 0.07 = (0.7/\sqrt{100})$ which is slightly degraded, and bias ≈ 0.0035 which is a reduction by about a factor of 30.
- (5) For a given E/N_0 and number of pulses integrated, the bias magnitude varies linearly with true target angle off-boresight (see Fig. 10).
- (6) In addition to the bias effects, the standard deviation of the estimates degrades as the true target angle increases off-boresight. At the edge of the beam, the degradation factor is about 1.4.

To make plausible a mechanism for how the bias arises, the following argument can be used. Consider a target on the positive side of boresight, near the edge of the beam. The sum- and difference-channel signals on a single pulse can then be visualized as parallel vectors of unit length, as shown in Fig. 11. To each of these vectors is added an independent Gaussian noise vector. If the SNR is near 0 dB, the rms length of these noise vectors is on the order of 1. (Strictly speaking, our convention has been that $E/N_0 = 0$ dB implies that the ratio of the noise quadrature components to the signal vector is 1, so that the ratio of the lengths of the noise and signal vectors is $\sqrt{2}$ at 0 dB.) The phase angle of the noise vector in each channel is uniformly distributed between $\pm\pi$.

The resultant phase angle in each channel varies (nonuniformly) over at least $\pm\pi/2$. The difference between the phase angles in the two channels, which is the argument of the cosine term in Eq. (3), is therefore random (although not uniformly distributed) over $\pm\pi$. The upshot is that there is significant probability of the cosine term being negative and producing estimates near -1 , while the target is located near $\theta = +1$. The result is to bias the estimate down from $+1$ to a lower value. Figure 12 shows how the probability of positive and negative estimates varies with E/N_0 and θ . While there is a higher probability of the estimate having the correct sign further from boresight, the effect of a sign reversal is greater, and the resultant bias magnitude is greater.



(a) Target halfway out of notch.



(b) Target at edge of notch.

Fig. 9(a-b). Incoherent integration.

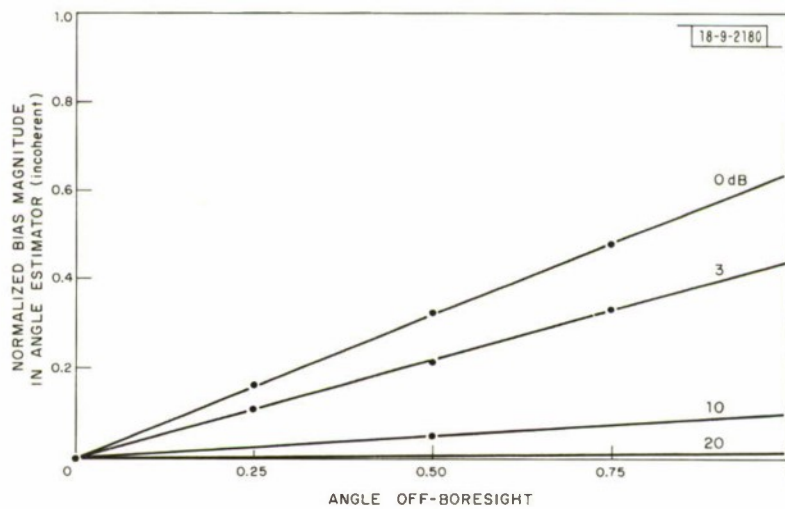


Fig. 10. Bias magnitude variation: 0- and 3-dB curves are independent of number of pulses; 10- and 20-dB curves are for 10 pulses or more (bias essentially disappears somewhere between 1 and 10 pulses at these E/N_0 's).

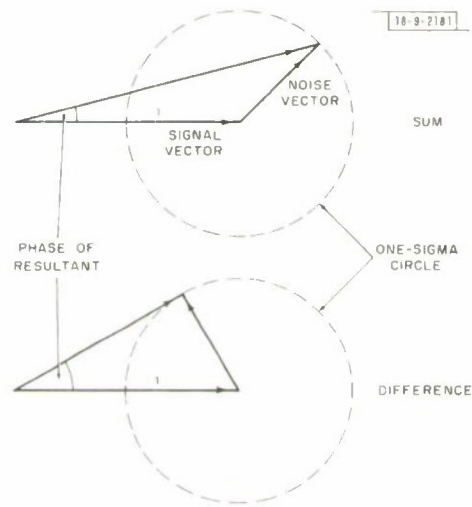


Fig. 11. Phase-angle geometry.

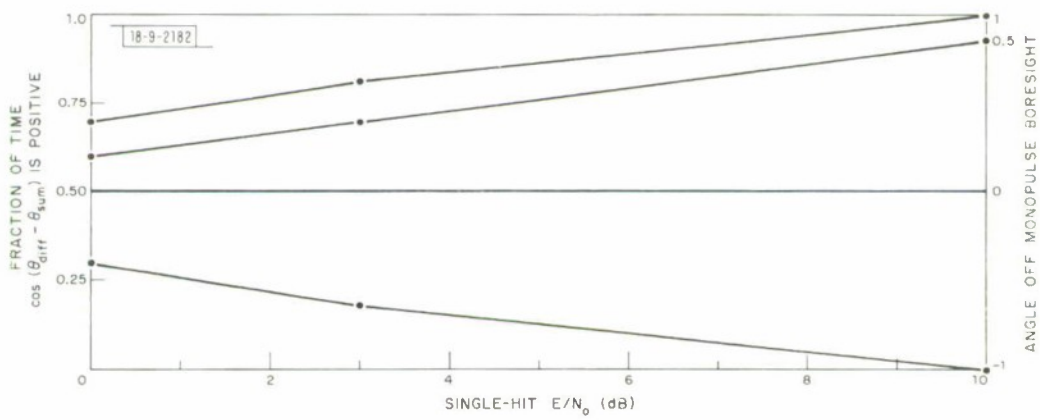


Fig. 12. Algebraic sign behavior of single-hit estimator.

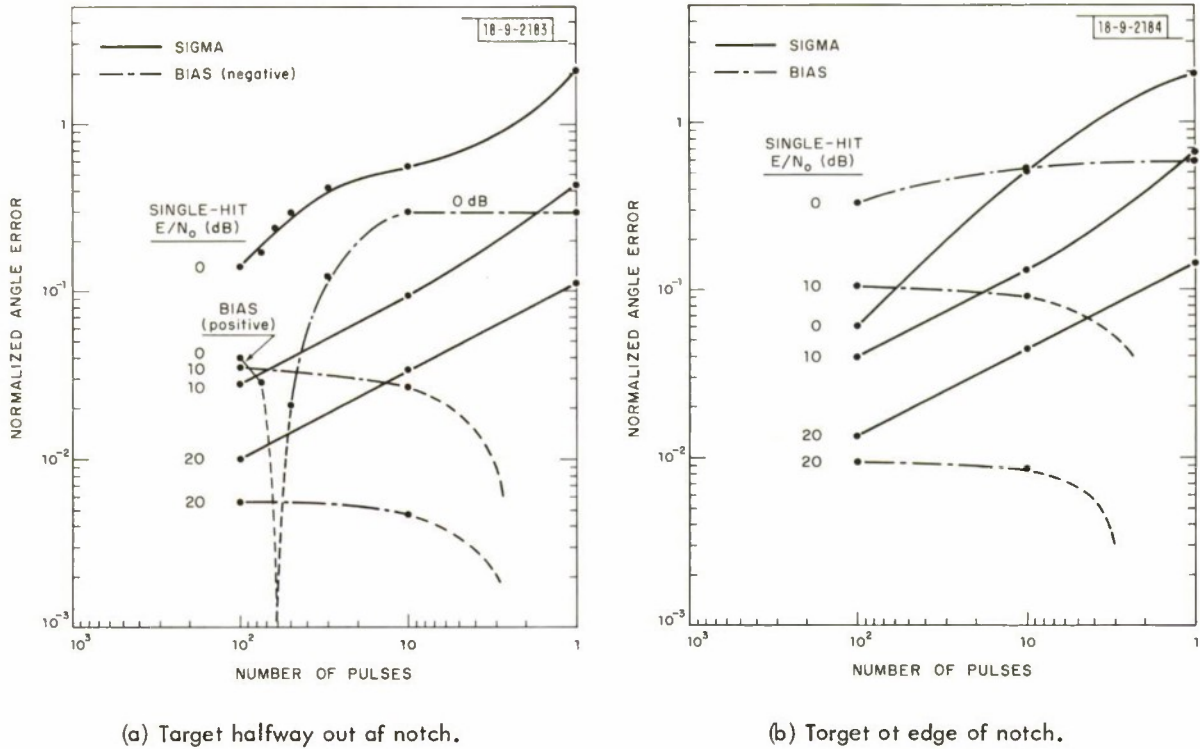


Fig. 13(a-b). Incoherent integration, majority rule phase estimator.

b. Majority Rule Sign Determination

Since the bias seemed to arise from the behavior of the phase angles on each pulse, a modified estimator was examined in which the sign of the estimate was determined by noting which sign occurred in a majority of the N pulses integrated. That is, the terms in the sum comprising the numerator in Eq. (3) were added with positive signs. The estimate was then made negative if more than half the terms had been negative individually. The resulting performance is shown in Figs. 13(a) and (b) for true target angles of 0.5 and 1, respectively. The results indicate that while the performance improves in certain respects, the modification is no panacea. We note that:

- (1) For a target halfway out from boresight ($\theta = 0.5$), there is little effect on the bias at 10 dB or above, where the bias is already relatively small. There is no effect on the precision. At 0 dB, the bias is driven down as the number of pulses is increased above 10. However, the precision is degraded, although not by the same factor. For example, at 50 pulses integrated, the bias is reduced by a factor of about 15 while the precision is degraded by a factor of about 3. At 10 pulses integrated, the bias is unchanged while the precision is degraded by a factor between 2 and 3. Furthermore, when enough pulses are integrated, the magnitude of the bias starts back up and the sign of the bias is changed (away from boresight).
- (2) For a target at the edge of the beam ($\theta = 1$), where the absolute magnitudes of the bias are greatest, there is essentially no effect at 10 dB or above. At 0 dB, there is a slight reduction in bias as the number of pulses is increased, amounting to a factor of 2 at 100 pulses. The precision is degraded by, at most, a factor of 2 at ~ 10 pulses, with less degradation as the number of pulses is reduced toward 1 or increased toward 100.

c. Effect of Bias

It is generally assumed that bias in an estimate is undesirable, and that ideally one wants an unbiased and consistent estimate. While this view seems reasonable, it does not preclude an analysis of any particular case to determine the effects of bias vs precision. It may be that the bias is removable in some way, or that its effect is unimportant. In Sec. 1, we limited the scope of this study to angle estimation, so that we have indicated the presence of bias in an angle estimate without commenting on its effect on angle tracking or track prediction. To determine its effect requires specifying algorithms for tracking or prediction. Without delving into this, we discuss below one simple example to exemplify such an analysis.

The example concerns angle tracking, or keeping the target in the beam. Consider a simple angle-tracking scheme which, after each estimate is made, centers the beam on the angle indicated by the latest estimate. Thus, if the latest estimate is $\hat{\Theta} = 0.5$ (target one-half beamwidth to the right of current pointing direction), the beam is moved one-half beamwidth to the right before making the next estimate. Assume that the basic approximate incoherent estimator is being used [Figs. 3, 9(a) and (b)], that E/N_0 is 0 dB, and that 100 pulses are integrated. Assume also that when the first detection and estimate are made, the beam happens to be pointed so that the target is located at $\Theta = 1$. For this situation, the precision is about 0.075 (less than a tenth of a beamwidth) and the bias is -0.6 , i.e., the mean of the estimate is 0.4. If the estimate were unbiased and had the same precision, the beam would immediately be centered on the true target angle \pm one-tenth of a beamwidth, with high probability. The beam would tend to remain centered, except for an occasional random kick-out, after which it would immediately be recentered with high probability. With the bias present, the beam would be moved to the right 0.4 unit with high probability after the first estimate. Thus, the bias in the second estimate would be -0.36 (true $\Theta = 0.6$, bias = -0.6Θ); after the second estimate, the beam would be moved about 0.24 unit to the right, placing the target 0.36 unit to the right of center. Continuing this sequence, we see that the complete sequence of angle offsets (true target angle relative to beam center) would be

$$1, 0.6, 0.36, 0.22, 0.13, 0.08, \dots$$

smearred by the zero mean component of the error. In the absence of bias, the sequence would be

$$1, 0, 0, 0, 0, 0, \dots$$

smearred by the zero mean component. Thus, whenever the target is located near the edge of the beam, the effect of the bias is to increase the time required to center the beam on the target. The self-centering action of the tracking loop appears to minimize the steady-state effect of the bias.

B. Maximum-Likelihood Estimator

1. On-Boresight Results

The basic performance of the maximum-likelihood estimator when the true target angle is zero is shown in Fig. 14. We note that:

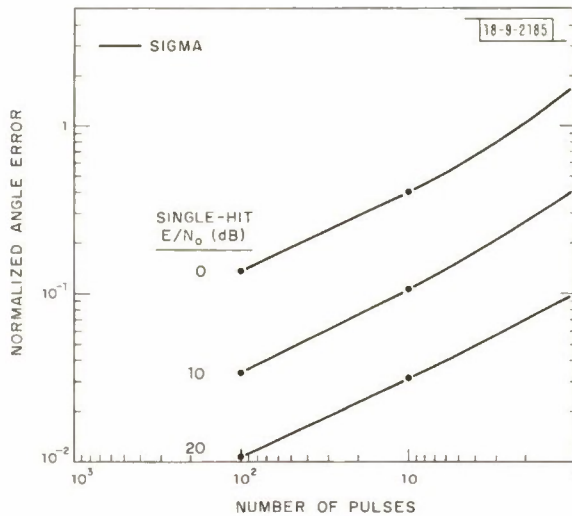


Fig. 14. Optimum (angle search) incoherent estimator, target on monopulse boresight.

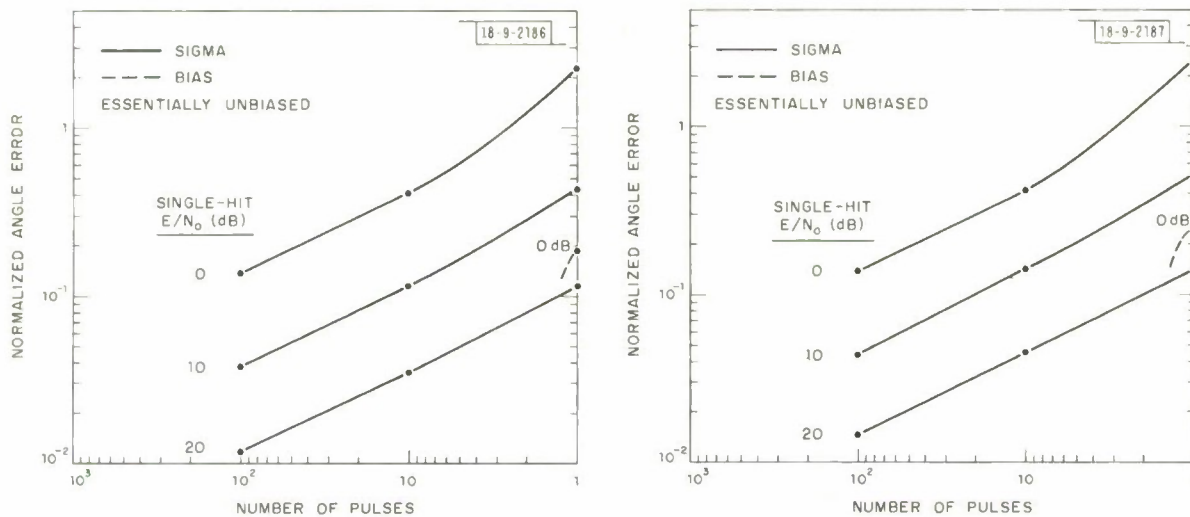
- (1) The estimate is unbiased.
- (2) At 10 dB or more, the precision is essentially equal to the precision of the approximate estimator, with the approximate estimator being slightly superior.
- (3) At 0 dB, the approximate estimator is superior by an amount which increases as the number of pulses increases, exceeding a factor of 2 at 100 pulses.

The fact that the approximate estimator outperforms the estimator it is approximating concerns the off-boresight performance of these estimators. Section III-C below, dealing with the theoretical bounds to the precision of the estimators, will support the simulation results. Briefly, there are two factors that support these results. First is the fact that the maximum-likelihood estimate in the incoherent case, while "asymptotically unbiased," is not "asymptotically efficient," i.e., does not have a precision converging to the Cramér-Rao bound for unbiased estimates as N increases. Second, because of its off-axis bias, the approximate incoherent estimator is not constrained to lie above the same bound which is obeyed by the maximum-likelihood estimate. In fact, the relevant bound on the approximate estimator is lower. These two facts leave theoretical room to admit the simulation results.

2. Off-Boresight Results

Figures 15(a) and (b) show the performance of the estimator when the target is located off-boresight at angles of 0.5 and 1, respectively. We note that:

- (1) The estimates are essentially unbiased. At 0 dB, there is a slight bias in the single-pulse estimate, which disappears as pulses are integrated and is undetectable at 10 pulses. At 10 dB or more, there is no bias detectable even in the single-pulse estimate.
- (2) The precision again converges to that of the approximate estimate as E/N_0 is increased, with virtually no difference at 20 dB and a slight advantage to the approximate estimate at 10 dB.
- (3) At 0 dB, the approximate estimator is again superior by an amount which grows to about a factor of 2 at 100 pulses.



(a) Target halfway out of notch.

(b) Target at edge of notch.

Fig. 15(a-b). Optimum (angle search) incoherent estimator.

C. Theoretical Bounds on Precision

The results presented thus far were obtained by simulation. This was dictated by the fact that it was not feasible to compute statistics of the estimators analytically. However, it is feasible to compute lower bounds to the precision of the estimates which are unbiased at any value of θ analytically. It is also possible to compute lower bounds on precision for the estimates which are biased off-boresight using a combination of analysis and the bias results from the simulation. It is desirable to compute these bounds as a check, to show that the simulation results obey the bounds and converge to them as limits. We defer a detailed description of the analysis to Appendix B, and present in this section the results of the analysis.

1. Bounds on Maximum-Likelihood Incoherent Estimator

In Appendix B, we show that the precision (standard deviation) of this (or any) unbiased estimator is bounded from below by

$$\sigma_{\theta} \geq \left[\frac{1}{N} \frac{1}{E/N_0} (1 + \theta^2) \right]^{1/2} \quad (7)$$

where N is the number of pulses integrated, E/N_0 is the SNR, and θ is the true target angle off-boresight. This bound is plotted in Fig. 16. Comparison with Figs. 14 and 15(a) and (b) shows the essential agreement of the simulation results with the bounds. We note that:

- (1) The simulation results lie above the bounds at 0 dB, move closer at 10 dB, and are essentially converged to the bounds at 20 dB, for any N .
- (2) The precision does not converge to the bound as N is increased when E/N_0 is small (compare at 0 dB, 100 pulses). That is, the maximum-likelihood estimator is not asymptotically efficient in this case. The subtlety responsible for this result is that the N observations are not identically distributed. Each sample contains a distinct phase shift ψ_k , and therefore a different mean (see Appendices A and B). The proof that maximum-likelihood estimates are asymptotically normal, unbiased, and efficient depends on the assumption that the samples are identically distributed.²

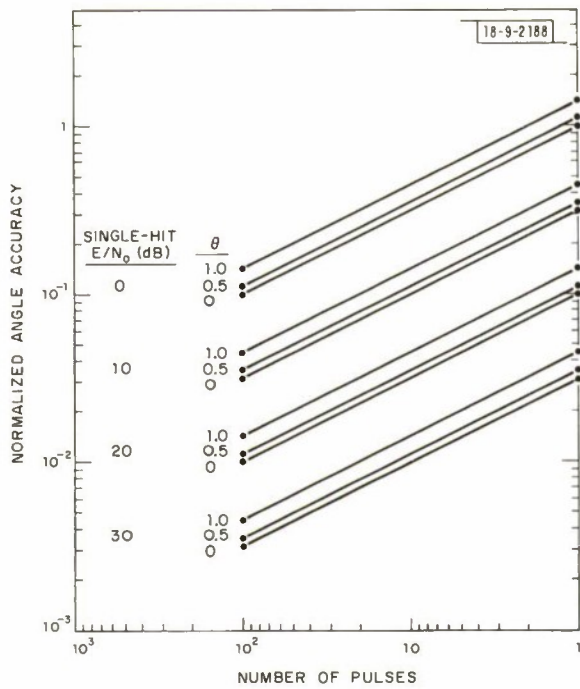
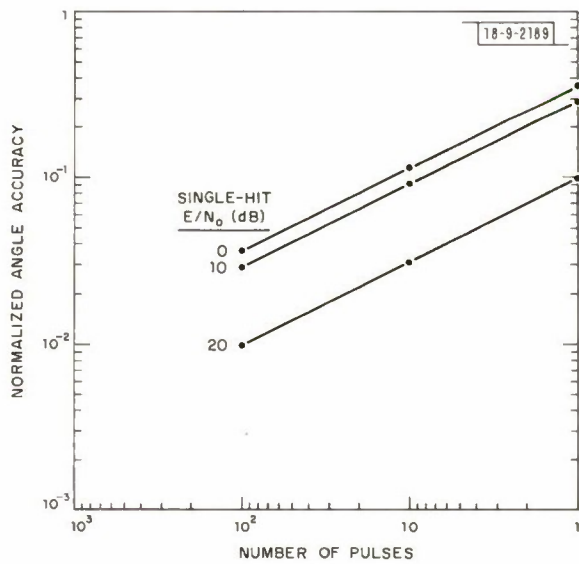
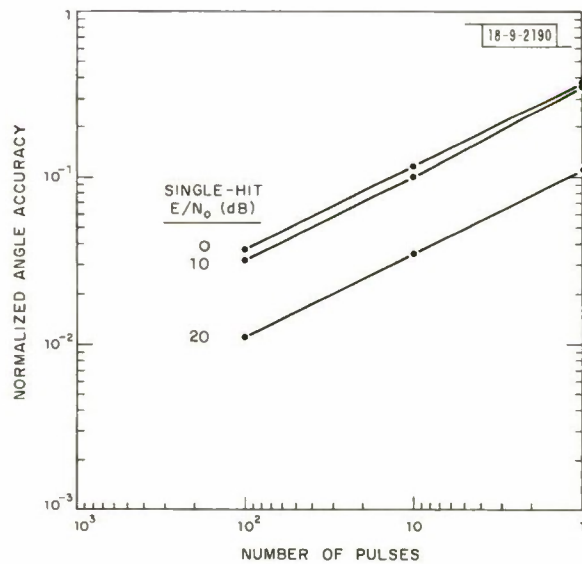


Fig. 16. Cramér-Rao bound, optimum (maximum-likelihood) incoherent estimator (or any unbiased estimator).



(a) $\theta = 0$ (on-baresight).



(b) $\theta = 0.5$.

Fig. 17(a-c). Cramér-Rao bounds, approximate incoherent estimator.

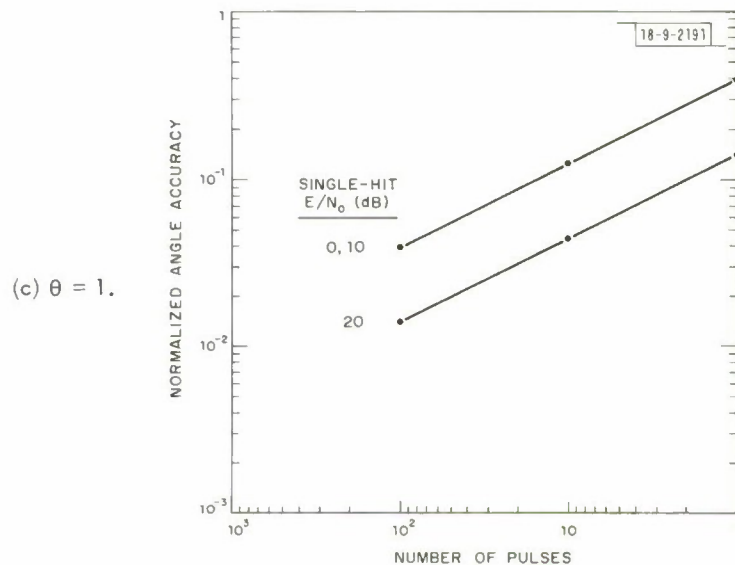


Fig. 17(a-c). Continued.

2. Bounds on Approximate Incoherent Estimator

This bound is more complicated to obtain, and requires a knowledge of the bias variation vs angle of the estimator. The presence of bias affects the bound even for $\theta = 0$, the angle at which the estimator is unbiased. In Appendix B, the bias data from the simulation are combined with analysis to produce the bounds shown in Figs. 17(a) through (c) ($\theta = 0, 0.5$, and 1 , respectively). These should be compared with Figs. 3, 9(a) and (b), respectively. We note that:

- (1) On-boresight, the simulation results lie above the bounds at 0 dB, move closer as E/N_0 is increased, and are essentially converged at 20 dB.
- (2) If the simulation results were compared with the bounds in Fig. 16, i.e., with bounds computed disregarding the off-axis bias, the results would appear to violate the bounds (compare Figs. 16 and 3 at 0 dB and 100 pulses).
- (3) Off-boresight, the results again satisfy the bounds, and converge to them as E/N_0 is increased to 20 dB.
- (4) At all angles, as E/N_0 is increased the bounds approach those for the unbiased estimator shown in Fig. 16, in agreement with the decrease in bias as E/N_0 is increased in Figs. 9(a) and (b).
- (5) As with the maximum-likelihood estimate, the precision does not approach the bound for low E/N_0 and large N .

IV. COHERENT PROCESSING

A. Approximate Estimator

1. On-Boresight Results

The basic performance of the approximate coherent estimator on-boresight is shown in Fig. 18. We note that:

- (1) The estimate is unbiased.
- (2) At SNRs of 10 dB or more, the precision is essentially identical to that of the approximate incoherent estimator. That is, there is no difference between coherent and incoherent processing in how the precision improves with E/N_0 or N . In both cases, there is a limiting inverse square-root dependence.

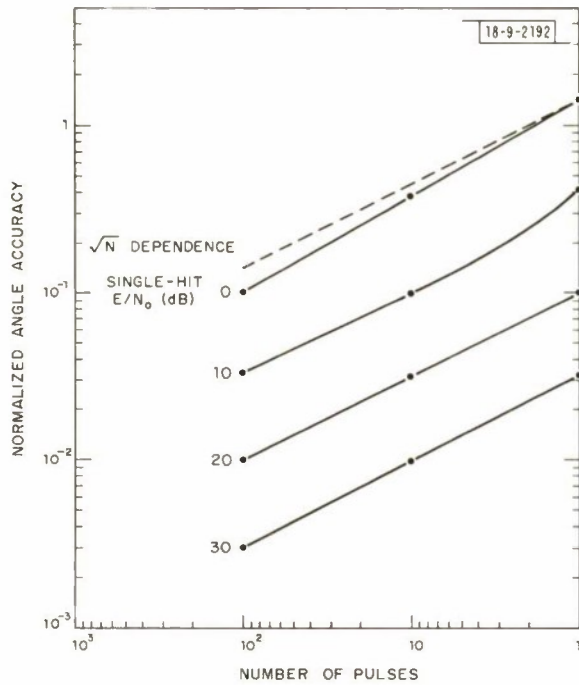
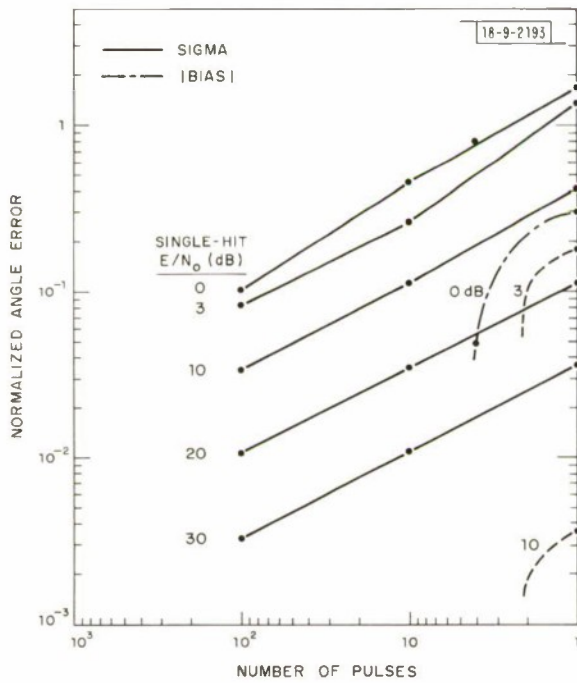
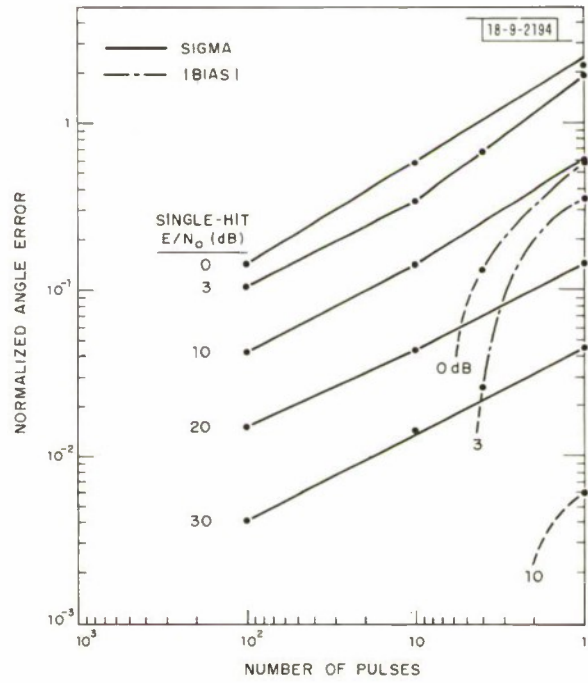


Fig. 18. Coherent integration, target on manapulse boresight.



(a) Target halfway out of notch.



(b) Target at edge of notch.

Fig. 19(a-b). Coherent integration.

- (3) At 0 dB, the precision is inferior to that of the incoherent estimator. At 100 pulses, the coherent precision is about halfway between that of the approximate incoherent estimate (Fig. 3) and the maximum-likelihood incoherent estimate (Fig. 14). As mentioned in Sec. III-B-1, recall that in the incoherent case the bound on an unbiased estimator falls below the maximum-likelihood performance and above the bound on the approximate estimator. As will be seen below in Secs. IV-B and -C and Appendix B, the bound on an unbiased estimate is the same in the coherent and incoherent cases, and the approximate coherent estimator is unbiased and asymptotically efficient and hence converges to this bound. This accounts for the value of the coherent precision relative to that of the incoherent estimates.

2. Off-Boresight Results

The performance at true target angles of 0.5 and 1 is shown in Figs. 19(a) and (b). We note that:

- (1) The single-pulse estimate is again biased, since it is identical to the incoherent single-pulse estimate. However, the bias rapidly drops off as pulses are integrated, and is undetectable at 10 pulses, even at an E/N_0 of 0 dB. The big advantage of coherent processing is the behavior of the bias, not the behavior of the precision. In terms of the phase-angle reasoning of Sec. III-A-2-a, the reason for the disappearance of the bias lies in how the carrier phase angle ψ is being estimated. Since the argument of the coherently summed samples in the sum channel is being used to estimate ψ , the uncertainty in ψ at low E/N_0 rapidly drops from $\pm\pi$ to near zero as pulses are integrated. Since the cosine term in the coherent estimator is $\cos(\varphi_{1k} - \hat{\psi})$, only the uncertainty in φ_{1k} , $\pm\pi/2$, remains after integration. Thus, the probability of a negative sign drops, and the bias vanishes.
- (2) As with incoherent processing, the precision degrades off-boresight, the degradation factor reaching 1.4 at $\Theta = 1$. The coherent and incoherent precisions are essentially identical above 10 dB.

3. Effect of Phase Errors

The coherent estimates are based on the assumption that the unknown target phase angle is constant over the set of pulses integrated. We examined the effects of two types of phase errors on the performance of the approximate coherent estimator on-boresight.

a. Random Pulse-to-Pulse Jitter

This type of phase error could represent an oscillator instability, target glint, etc. Figures 20(a) and (b) show the effects of phase jitter uniformly distributed between $\pm\pi/2$ (rms jitter = 52°) and $\pm\pi$ (rms jitter = 104°), respectively. We note that:

- (1) There is a surprising tolerance to the 90° jitter, i.e., there is still an "integration gain," although it is somewhat reduced. The reduction in integration gain is roughly independent of E/N_0 . For example [see Figs. 18 and 20(a)], at 0 dB the integration gain for 100 pulses is 14 without jitter and 8.5 with jitter, a degradation factor of 1.65. At 20 dB, the integration gain is 10 without jitter and 6.45 with jitter, a degradation factor of 1.55.
- (2) The 180° jitter wipes out any benefits of integration. Precision is equal to or worse than the single-pulse precision for any number of pulses integrated up to 100, at any SNR.

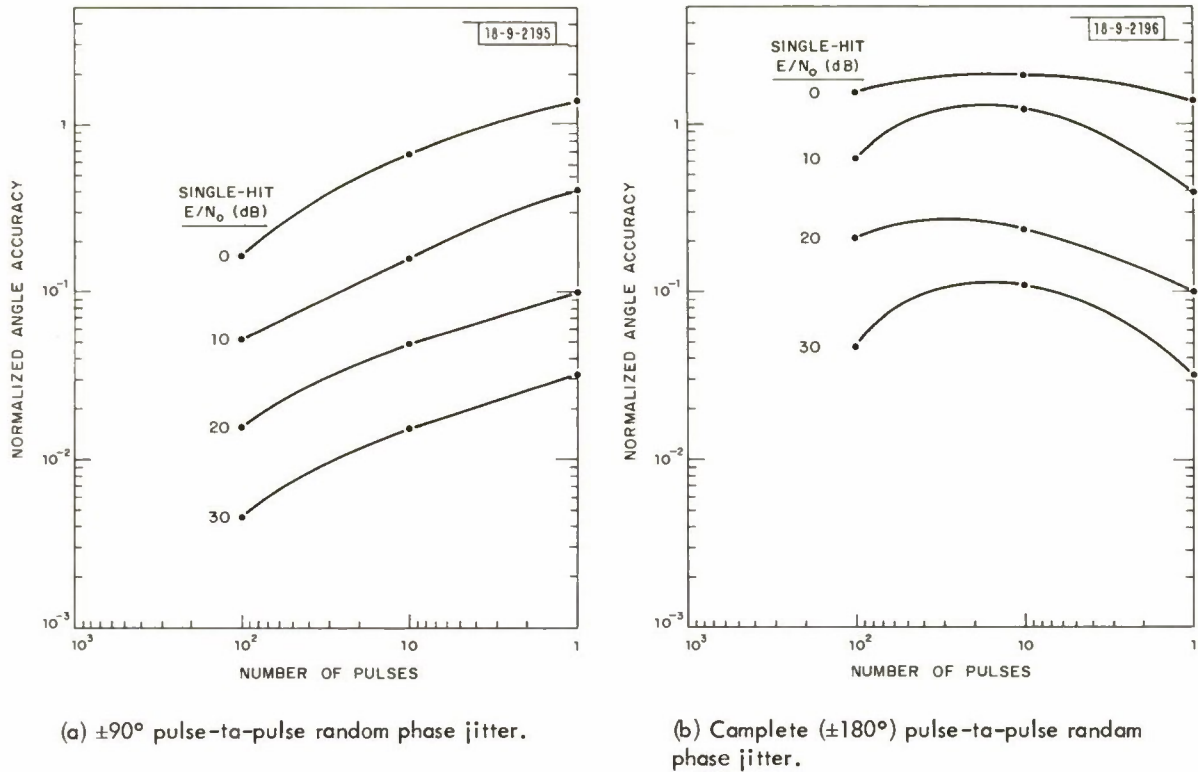
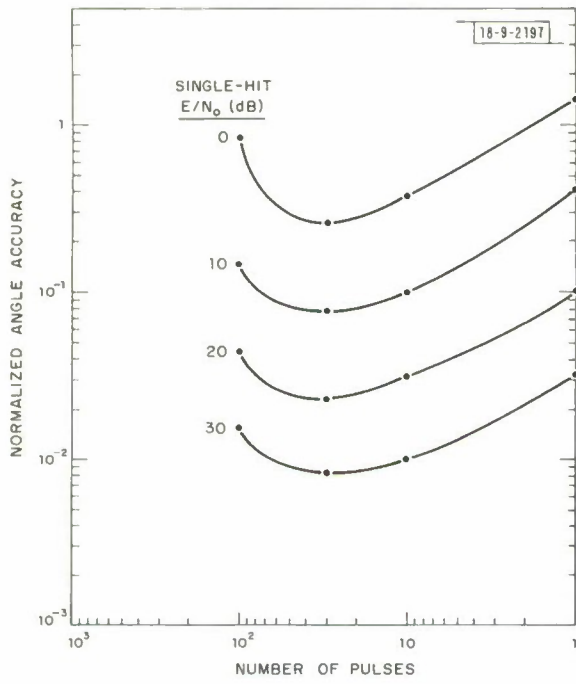


Fig. 20(a-b). Coherent integration, target on-boresight.

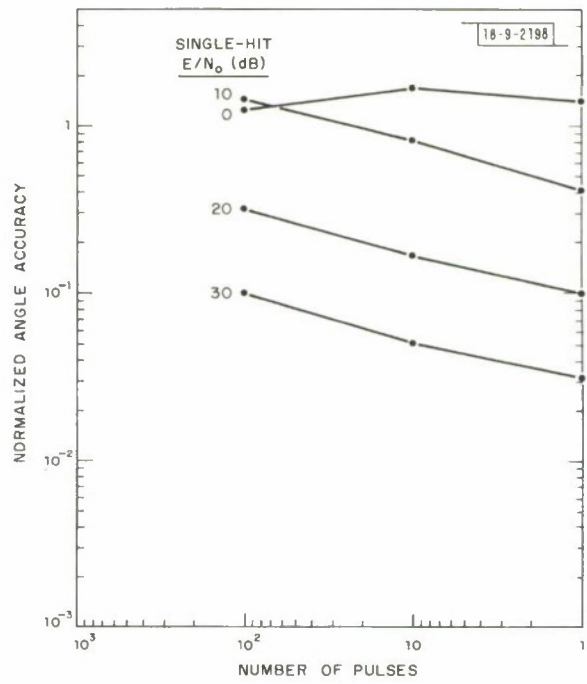
b. Systematic Pulse-to-Pulse Drift

The angle estimators were derived assuming that the carrier frequency of the target return was known. If the target doppler shift is not known perfectly, the effect will be to introduce a systematic phase progression into the sequence of pulses being integrated. Typically, a receiver might be set up with a bank of doppler filters, be they offset filters, staggered oscillators, etc., with responses crossing over at about the doppler resolution of the radar signal. Thus, a target may be offset in doppler anywhere between zero and the doppler resolution with respect to the peak of the closest doppler channel. An offset relative to the center of a doppler channel introduces an equivalent phase drift between pulses. If no further doppler processing is done in the radar to refine the doppler accuracy to better than the resolution, the phase shifts can be significant. Figures 21(a) through (c) show the effects of systematic interpulse phase shifts of 5° , 30° , and 90° , respectively, on the precision of the coherent estimator on-boresight. We note that:

- (1) Only 5° of phase shift is enough to halt the improvement of precision vs number of pulses at $N = 30$, and to degrade the precision beyond that point.
- (2) With 30° of phase shift, there is no integration gain at all. For E/N_0 of 10 dB or more, the precision degrades from its single-pulse value as N is increased. At 0 dB, the precision is essentially independent of N .
- (3) With 90° of phase shift, the rate of degradation is accentuated, and is more pronounced at the higher SNRs.



(a) 5° systematic pulse-to-pulse phase drift.



(b) 30° systematic pulse-to-pulse phase drift.

(c) 90° systematic pulse-to-pulse phase drift.

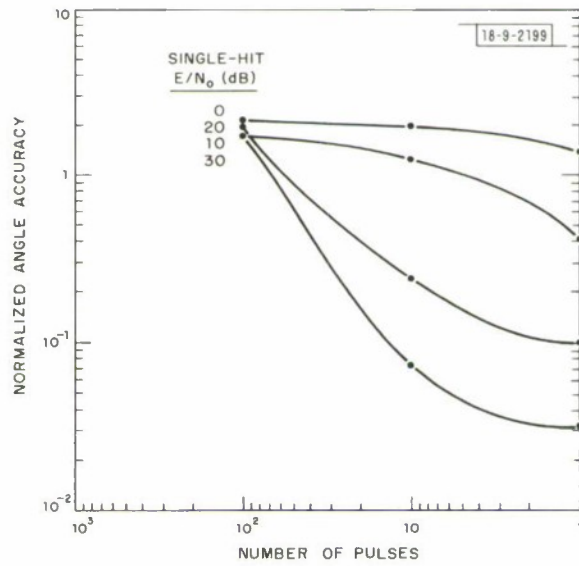


Fig. 21(a-c). Coherent integration, target on-baresight.

B. Maximum-Likelihood Estimator

Figure 22 shows the performance of the maximum-likelihood coherent estimator on-boresight. Comparison with Fig. 18 reveals that the performance is virtually identical to that of the approximate estimator. While we have not run this estimator off-boresight, it coincides with the incoherent maximum-likelihood estimator at 1 pulse, and thus has less bias than the approximate

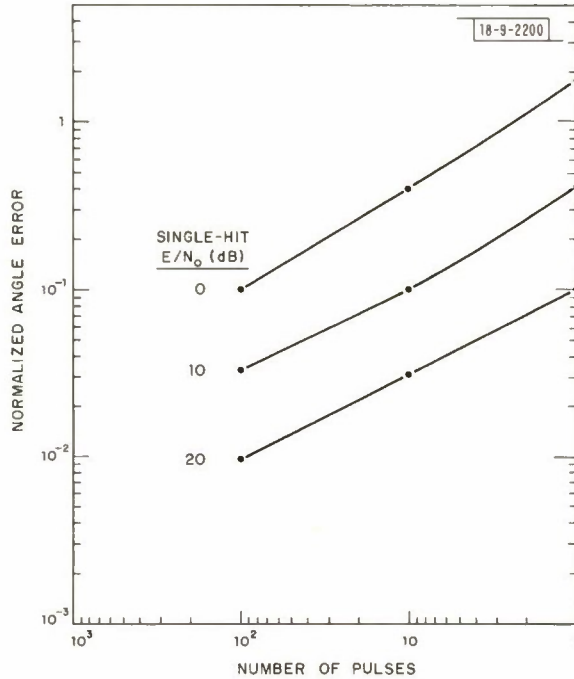


Fig. 22. Optimum (angle-search) estimator, coherent case, target on monopulse boresight.

coherent estimator at 1 pulse off-boresight [see Figs. 15(b) and 19(b)]. The bias drops off so quickly with N for the approximate coherent estimator that there is no reason to use the exact estimator with its required search in the coherent case.

C. Theoretical Bounds on Precision

We have seen above that the approximate estimator is unbiased at any value of θ or E/N_0 , once a few pulses are integrated. Thus, certainly for 10 pulses or above, we can compare the results of Figs. 18 and 19(a) and (b) with the bounds of Fig. 16 which apply to any unbiased estimator of θ . The results essentially obey the bounds and converge to them not only for high E/N_0 , as in the incoherent case, but also for large N at low E/N_0 . That is, the coherent estimator is asymptotically efficient even for low-per-pulse E/N_0 . In the coherent case, the N observations all contain a common phase shift ψ , and are therefore identically distributed. The maximum-likelihood estimator is then asymptotically efficient, and must converge to the bounds of Fig. 16 as N increases, even when E/N_0 is low.

APPENDIX A
MONOPULSE ANGLE ESTIMATORS

This Appendix describes the derivation of the maximum-likelihood-angle estimates and their approximations, and is abstracted from Ref. 1.

Consider a set of b beams, each containing a filter matched to the pulse shape, range, and doppler of the target of interest. On each radar pulse, the matched-filter output is sampled at the time of peak output due to target. The complex number or sample obtained in the i^{th} beam on the k^{th} pulse is then

$$y_{ik} = A e^{j\psi_k} G_i(\theta, \varphi) + n_{ik} \quad , \quad 1 \leq i \leq b \quad , \quad 1 \leq k \leq N \quad . \quad (\text{A-1})$$

A and ψ_k are the amplitude and phase of the output due to target, A being independent of k . A coherent case is defined in which $\psi_k = \psi$ independent of k , for all k . An incoherent case is defined in which the k phase values ψ_k are k distinct parameters. The function $G_i(\theta, \varphi)$ specifies the shape of the i^{th} beam as a function of the two spatial angles θ and φ . The complex noise sample n_{ik} is composed of quadrature components as

$$n_{ik} = n_{ikc} + jn_{iks} \quad (\text{A-2})$$

where the quadrature components are assumed to be zero mean real Gaussian variates with known variance σ^2 independent of k . The noise is assumed independent from beam-to-beam and from pulse-to-pulse.

Define b -dimensional column vectors as

$$\underline{y}_k^T = [y_{1k} \dots y_{bk}]$$

$$\underline{n}_k^T = [n_{1k} \dots n_{bk}]$$

$$\underline{G}^T(\theta, \varphi) = [G_1(\theta, \varphi) \dots G_b(\theta, \varphi)]$$

an N -dimensional vector $\underline{\psi}^T = [\psi_1 \dots \psi_N]$, and the $b \times b$ diagonal covariance matrix

$$\Lambda_o = E(\underline{n}_k \underline{n}_k^T) = 2\sigma^2 I_b$$

where T denotes transposition, $*$ indicates complex conjugation, and I_b is the $b \times b$ unit matrix. We can write the probability of the received samples on the k^{th} pulse given values of A , ψ_k , θ , and φ as

$$p(\underline{y}_k / A, \psi_k, \theta, \varphi) = \frac{1}{\pi^b |\Lambda_o|} \exp \left[- \left(\underline{y}_k - A e^{j\psi_k} \underline{G} \right)^T \Lambda_o^{-1} \left(\underline{y}_k - A e^{j\psi_k} \underline{G} \right) \right] \quad (\text{A-3})$$

where

$$|\Lambda_o| = \text{determinant}(\Lambda_o) = (2\sigma^2)^b \quad . \quad (\text{A-4})$$

The conditional probability of receiving the total set of data $\underline{y}_1 \dots \underline{y}_N$ is then

$$p(\underline{y}_1 \dots \underline{y}_N / A, \underline{\psi}, \Theta, \varphi) = \frac{1}{\pi^{Nb} |\Lambda_o|} \exp \left[- \sum_{k=1}^N \left(\underline{y}_k - A e^{j\psi} \underline{k} \underline{G} \right)^{T*} \Lambda_o^{-1} \left(\underline{y}_k - A e^{j\psi} \underline{k} \underline{G} \right) \right] . \quad (\text{A-5})$$

The likelihood-ratio L is the ratio of this probability to that of receiving the data given no target ($A = 0$), and can be written as

$$L = \exp \left\{ \sum_{k=1}^N \left[- \left(\underline{y}_k - A e^{j\psi} \underline{k} \underline{G} \right)^{T*} \Lambda_o^{-1} \left(\underline{y}_k - A e^{j\psi} \underline{k} \underline{G} \right) + \underline{y}_k^{T*} \Lambda_o^{-1} \underline{y}_k \right] \right\} . \quad (\text{A-6})$$

We want to solve for the values of A , $\underline{\psi}$, Θ , and φ which jointly maximize L , and use the resultant values $\hat{\Theta}$ and $\hat{\varphi}$ as estimates of the spatial angles Θ and φ . L will be maximized if we maximize the quantity

$$\frac{2}{N} \operatorname{Re} \left(\sum_{k=1}^N \underline{y}_k^T \Lambda_o^{-1} A e^{-j\psi} \underline{k} \underline{G} \right) - A^2 \underline{G}^T \Lambda_o^{-1} \underline{G} . \quad (\text{A-7})$$

If we define

$$\underline{w} = \operatorname{Re} \left(\frac{1}{N} \sum_{k=1}^N \underline{y}_k e^{-j\psi} \underline{k} \right) \quad (\text{A-8})$$

we want to maximize

$$2A \underline{w}^T \Lambda_o^{-1} \underline{G} - A^2 \underline{G}^T \Lambda_o^{-1} \underline{G} . \quad (\text{A-9})$$

Differentiating with respect to A yields a maximizing value of A as

$$\hat{A} = \frac{\underline{w}^T \Lambda_o^{-1} \underline{G}}{\underline{G}^T \Lambda_o^{-1} \underline{G}} . \quad (\text{A-10})$$

Substituting back into expression (A-9), we obtain the remaining maximization

$$\max_{\underline{\psi}, \Theta, \varphi} \left[\frac{(\underline{w}^T \Lambda_o^{-1} \underline{G})^2}{\underline{G}^T \Lambda_o^{-1} \underline{G}} \right] \quad (\text{A-11})$$

which, upon substitution of Eq. (A-8), becomes

$$\max_{\underline{\psi}, \Theta, \varphi} \left\{ \frac{\left[\frac{1}{N} \sum_{k=1}^N \operatorname{Re} \left(\underline{y}_k^T \Lambda_o^{-1} \underline{G} e^{j\psi} \underline{k} \right) \right]^2}{\underline{G}^T \Lambda_o^{-1} \underline{G}} \right\} . \quad (\text{A-12})$$

In the incoherent case, we will obtain a maximum with respect to $\underline{\psi}$ if each term within the real part operator is made real, i.e., if

$$\psi_k = -\arg \left(\underline{y}_k^T \Lambda_o^{-1} \underline{G} \right) . \quad (\text{A-13})$$

This leaves us with a maximization

$$\max_{\Theta, \varphi} \frac{\left(\sum_{k=1}^N |y_k^T \Lambda_o^{-1} \underline{G}| \right)^2}{\underline{G}^T \Lambda_o^{-1} \underline{G}} \quad (\text{A-14})$$

which defines the desired angle estimates $\hat{\Theta}$ and $\hat{\varphi}$.

In the coherent case, expression (A-12) will be maximized if

$$\psi_k = \psi = -\arg \left(\sum_{k=1}^N y_k^T \Lambda_o^{-1} \underline{G} \right) , \quad \text{all } k \quad (\text{A-15})$$

which leaves a maximization

$$\max_{\Theta, \varphi} \frac{\left| \sum_{k=1}^N y_k^T \Lambda_o^{-1} \underline{G} \right|^2}{\underline{G}^T \Lambda_o^{-1} \underline{G}} \quad (\text{A-16})$$

defining the desired angle estimates $\hat{\Theta}$ and $\hat{\varphi}$.

In the special case of a single spatial angle Θ and two beams, one constant vs Θ and the other linear in Θ , so that

$$b = 2 \quad , \quad \underline{G}^T(\Theta) = [\Theta, 1] \quad (\text{A-17})$$

expressions (A-14) and (A-16) reduce to the exact estimators of Sec. II, Eqs. (1) and (2).

To obtain approximations to these estimators, we backtrack to expression (A-11), and maximize it first with respect to Θ and φ , holding \underline{w} (that is $\underline{\psi}$) fixed. Applying the Schwartz inequality for vectors to (A-11) results in

$$\frac{(\underline{w}^T \Lambda_o^{-1} \underline{G})^2}{\underline{G}^T \Lambda_o^{-1} \underline{G}} \leq \underline{w}^T \Lambda_o^{-1} \underline{w} \quad (\text{A-18})$$

Equality is achieved in this expression only if a scalar α can be found such that

$$\underline{G} = \alpha \underline{w} \quad (\text{A-19})$$

Assuming that the functional form of \underline{G} is such that Eq. (A-19) can be satisfied for any \underline{w} , the remaining maximization becomes

$$\max_{\underline{\psi}} \underline{w}^T \Lambda_o^{-1} \underline{w} \quad (\text{A-20})$$

Without specifying how this operation is explicitly performed, we can denote the maximizing set of phases by

$$\underline{\hat{\psi}}^T = [\hat{\psi}_1 \dots \hat{\psi}_N] \quad (\text{A-21})$$

in terms of which Eq. (A-19) specifies the resultant spatial angle estimates $\hat{\Theta}$ and $\hat{\varphi}$ as

$$\underline{G}(\hat{\Theta}, \hat{\varphi}) = \alpha \hat{\underline{w}} = \alpha \operatorname{Re} \left(\frac{1}{N} \sum_{k=1}^N y_k e^{-j\hat{\psi}_k} \right) \quad (\text{A-22})$$

If we now assume two beams, and one spatial angle Θ , Eq. (A-22) becomes

$$\frac{G_1(\hat{\Theta})}{G_2(\hat{\Theta})} = \frac{\operatorname{Re} \sum_{k=1}^N y_{1k} e^{-j\hat{\psi}_k}}{\operatorname{Re} \sum_{k=1}^N y_{2k} e^{-j\hat{\psi}_k}} \quad (\text{A-23})$$

where G_1 and G_2 are the scalar patterns of the two beams. To proceed, we must make explicit how the phase estimates $\hat{\psi}$ are to be made. If we think of G_1 as representing a difference beam, and G_2 a sum beam, it seems as reasonable as anything else to use the phase angle of the sum beam sample as the estimate $\hat{\psi}_k$ on each pulse in the incoherent case. That is,

$$\hat{\psi}_k = \arg(y_{2k}) \quad . \quad (\text{A-24})$$

Equation (A-23) then becomes

$$\frac{G_1(\hat{\Theta})}{G_2(\hat{\Theta})} = \frac{\sum_{k=1}^N |y_{1k}| \cos(\varphi_{1k} - \varphi_{2k})}{\sum_{k=1}^N |y_{2k}|} \quad (\text{A-25})$$

where

$$\begin{aligned} \varphi_{1k} &= \arg(y_{1k}) \\ \varphi_{2k} &= \arg(y_{2k}) \quad . \end{aligned} \quad (\text{A-26})$$

Finally, assuming that

$$\underline{G}^T(\Theta) = [\Theta, 1] \quad (\text{A-27})$$

[which satisfies Eq. (A-19)], results in the explicit approximate incoherent estimator:

$$\hat{\Theta} = \frac{\sum_{k=1}^N |y_{1k}| \cos(\varphi_{1k} - \varphi_{2k})}{\sum_{k=1}^N |y_{2k}|} \quad . \quad (\text{A-28})$$

In the coherent case, it seems reasonable to take the phase estimate $\hat{\psi}$ as the phase of the coherently summed samples in the sum beam. That is,

$$\hat{\psi} = \arg \left[\sum_{k=1}^N y_{2k} \right] \quad . \quad (\text{A-29})$$

The resultant explicit approximate coherent estimator is:

$$\hat{\Theta} = \frac{\sum_{k=1}^N |y_{1k}| \cos(\varphi_{1k} - \hat{\psi})}{\left| \sum_{k=1}^N y_{2k} \right|} \quad . \quad (\text{A-30})$$

Equations (A-28) and (A-30) match Eqs. (3) and (4) in Sec. II.

APPENDIX B
THEORETICAL BOUNDS TO ESTIMATOR PRECISION

Theoretical bounds on the precision of an estimate can be obtained by starting with the matrix form of the Cramér-Rao inequality.³ This can be stated as follows.

Consider an a -dimensional vector of parameters $\underline{\alpha}$, and a vector estimate of $\underline{\alpha}$ denoted by $\hat{\underline{\alpha}}$. Let $\underline{m} = E(\hat{\underline{\alpha}})$ denote the expected value of the estimate $\hat{\underline{\alpha}}$. Define an $a \times a$ matrix Q as

$$Q = \frac{\partial \underline{m}}{\partial \underline{\alpha}} \tag{B-1}$$

that is, the i - j element of Q is

$$Q_{ij} = \frac{\partial m_j}{\partial \alpha_i} \tag{B-2}$$

where m_j and α_i are the scalar components of \underline{m} and $\underline{\alpha}$. Let p represent the conditional probability of the received data:

$$p = p(\underline{y}_1 \dots \underline{y}_N / \underline{\alpha}) \tag{B-3}$$

where $\underline{y}_1 \dots \underline{y}_N$ are the received or observed complex vector samples on N pulses or trials. The dimension of the vector \underline{y}_k is equal to the number of beams b in our case. In terms of p , define the $a \times a$ matrix Λ as

$$\Lambda = E \left[\left(\frac{\partial \ln p}{\partial \underline{\alpha}} \right) \left(\frac{\partial \ln p}{\partial \underline{\alpha}} \right)^T \right] \tag{B-4}$$

where $\partial \ln p / \partial \underline{\alpha}$ is an a -dimensional column vector whose k^{th} element is $\partial \ln p / \partial \alpha_k$.

The Cramér-Rao inequality states that the covariance matrix of the estimate $\hat{\underline{\alpha}}$ obeys

$$C = E[(\hat{\underline{\alpha}} - \underline{m})(\hat{\underline{\alpha}} - \underline{m})^T] \geq Q^T \Lambda^{-1} Q \tag{B-5}$$

where the inequality sign denotes positive definiteness.[†] In particular, if we are interested in the variance of a particular component of $\hat{\underline{\alpha}}$, Eq. (B-5) implies that the appropriate diagonal element of C is greater than or equal to the corresponding element of $Q^T \Lambda^{-1} Q$.

Note that the inequality depends on the mean or expected value of $\hat{\underline{\alpha}}$. If the estimate $\hat{\underline{\alpha}}$ is unbiased, then

$$\underline{m} = \underline{\alpha} \tag{B-6}$$

and Q becomes a unit matrix. The inequality

$$C \geq \Lambda^{-1} \tag{B-7}$$

then applies to any unbiased estimate $\hat{\underline{\alpha}}$, and one can talk about the relative efficiency of two unbiased estimates in approaching the bound. If the estimate is biased at any value of the parameters $\underline{\alpha}$, then the bound cannot be computed unless the dependence of \underline{m} on $\underline{\alpha}$ is known.

[†] Equation (B-5) implies that the matrix $C - Q^T \Lambda^{-1} Q$ is non-negative definite.

Furthermore, any two biased estimators will, in general, have different bias performance. This means that the bound changes for each estimate, and one cannot talk about how closely the two estimates approach a common bound as in the unbiased case.

If one assumes that $\hat{\underline{\alpha}}$ is unbiased, at least for some values of E/N_o and N , we see then that the bound (B-7) can be used to get a lower bound on precision without running a simulation. The bound is valid if the assumption is correct. If one further assumes that $\hat{\underline{\alpha}}$ is "asymptotically efficient" for large enough E/N_o , and turns out to be correct, then the actual limiting value of the precision has been obtained with no simulation.

When $\hat{\underline{\alpha}}$ is biased, the bound has less utility. The bias behavior must be determined either by analysis or simulation. The bound then obtained can be used as a check on the performance determined by simulation.

We will obtain below the bounds on the unbiased estimators in the incoherent and coherent cases, and the bounds on the biased approximate incoherent estimator of Sec. III-A.

Consider first the matrix Λ . Assuming zero mean Gaussian noise, independent from beam-to-beam and from pulse-to-pulse, of known variance σ^2 (variance of real RF or IF noise and each of its quadrature components), allows us to write

$$p(\underline{y}_1 \dots \underline{y}_N / \underline{\alpha}) = \frac{1}{\pi^{bN} |\Lambda_o| N} \exp \left[- \sum_{k=1}^N (\underline{y}_k - \underline{\mu}_k)^{T*} \Lambda_o^{-1} (\underline{y}_k - \underline{\mu}_k) \right] \quad . \quad (\text{B-8})$$

Here, b is the number of beams; N is the number of pulses; $\underline{\alpha}$ is a parameter vector whose components are N phase angles ψ_k , target amplitude A , and spatial angle Θ in the incoherent case and a common phase angle ψ , A , and Θ in the coherent case; and $\underline{\mu}_k$ is the mean of the k^{th} vector observation

$$\underline{\mu}_k = E(\underline{y}_k) = A e^{j\psi_k} \underline{G}(\Theta) \quad . \quad (\text{B-9})$$

$\underline{G}(\Theta)$ is the vector of beam patterns, and the covariance matrix Λ_o is

$$\Lambda_o = 2\sigma^2 I_b \quad (\text{B-10})$$

i. e., $2\sigma^2$ times a unit matrix of dimension b .

Using Eq. (B-8) and recognizing conjugate terms, we obtain

$$\frac{\partial \ln p}{\partial \alpha_i} = 2 \operatorname{Re} \sum_{k=1}^N \frac{\partial \underline{\mu}_k^{T*}}{\partial \alpha_i} \Lambda_o^{-1} (\underline{y}_k - \underline{\mu}_k) = 2 \operatorname{Re} \sum_{k=1}^N \frac{\partial \underline{\mu}_k^{T*}}{\partial \alpha_i} \Lambda_o^{-1} \underline{n}_k \quad (\text{B-11})$$

where \underline{n}_k is the complex vector noise sample on the k^{th} pulse. From Eq. (B-4), the i - j element of Λ is

$$\Lambda_{ij} = E \left(\frac{\partial \ln p}{\partial \alpha_i} \frac{\partial \ln p}{\partial \alpha_j} \right) \quad .$$

Using Eq. (B-11) and the identity

$$\operatorname{Re} (AB) + \operatorname{Re} (AB^*) = 2 \operatorname{Re} (A) \operatorname{Re} (B) \quad , \quad A, B \text{ complex scalars} \quad (\text{B-12})$$

and using the assumed noise independence properties

$$E(\underline{n}_k \underline{n}_l^T) = 2\sigma^2 \delta_{kl} \quad , \quad E(\underline{n}_k \underline{n}_l^T) = 0 \quad (\text{B-13})$$

we obtain

$$\Lambda_{ij} = 2\text{Re} \sum_{k=1}^N \frac{\partial \underline{\mu}_k^T}{\partial \alpha_i} \Lambda_O^{-1} \frac{\partial \underline{\mu}_k}{\partial \alpha_j} \quad (\text{B-14})$$

Now, separate $\underline{\alpha}$ as

$$\begin{aligned} \underline{\alpha}^T &= [\underline{\gamma}, \psi_1, \dots, \psi_N] && \text{incoherent} \\ \underline{\alpha}^T &= [\underline{\gamma}, \psi] && \text{coherent} \end{aligned} \quad (\text{B-15})$$

where $\underline{\gamma}$ contains the non-phase angle components as

$$\underline{\gamma}^T = [A, \Theta] \quad (\text{B-16})$$

In these terms, the means $\underline{\mu}_k$ are given by

$$\underline{\mu}_k(\underline{\alpha}) = E(\underline{y}_k) = E(A e^{j\psi_k} \underline{G}(\Theta) + \underline{n}_k) = e^{j\psi_k} A \underline{G}(\Theta) = e^{j\psi_k} \underline{A}(\underline{\gamma}) \quad (\text{B-17})$$

Thus, the partial derivatives in Eq. (B-14) are

$$\begin{aligned} \frac{\partial \underline{\mu}_k}{\partial \psi_i} &= j \delta_{ik} e^{j\psi_k} \underline{A}(\underline{\gamma}) && i = 1, N \quad \text{incoherent} \\ \frac{\partial \underline{\mu}_k}{\partial \psi} &= j e^{j\psi} \underline{A}(\underline{\gamma}) && \text{coherent} \\ \frac{\partial \underline{\mu}_k}{\partial \gamma_i} &= e^{j\psi_k} \frac{\partial \underline{A}(\underline{\gamma})}{\partial \gamma_i} && i = 1, 2 \quad (\text{B-18}) \end{aligned}$$

Consider any Λ_{ij} for which α_i is an element of $\underline{\gamma}$, and α_j is a phase ψ_j . Any such term is zero because of the real part operator in Eq. (B-14) coupled with the $j = \sqrt{-1}$ in Eq. (B-18). If α_i and α_j both correspond to elements of $\underline{\gamma}$, we obtain

$$\Lambda_{ij} = 2N \frac{\partial \underline{A}^T(\underline{\gamma})}{\partial \gamma_i} \Lambda_O^{-1} \frac{\partial \underline{A}(\underline{\gamma})}{\partial \gamma_j} \quad (\text{B-19})$$

while if α_i and α_j correspond to phase angles ψ_i and ψ_j , we obtain

$$\begin{aligned} \Lambda_{ij} &= 2 \underline{A}^T(\underline{\gamma}) \Lambda_O^{-1} \underline{A}(\underline{\gamma}) \delta_{ij} && \text{incoherent} \\ \Lambda_{ii} &= 2N \underline{A}^T(\underline{\gamma}) \Lambda_O^{-1} \underline{A}(\underline{\gamma}) && \text{coherent} \end{aligned} \quad (\text{B-20})$$

Thus, the matrix Λ^{-1} is

$$\Lambda^{-1} = \left[\begin{array}{c|c} \begin{array}{l} 2 \times 2 \\ \text{i-j element is} \\ 2N \frac{\partial \underline{A}^T(\underline{\gamma})}{\partial \gamma_i} \Lambda_o^{-1} \frac{\partial \underline{A}(\underline{\gamma})}{\partial \gamma_j} \end{array} & \begin{array}{l} 2 \times N \\ \bigcirc \end{array} \\ \hline \begin{array}{l} N \times 2 \\ \bigcirc \end{array} & \begin{array}{l} N \times N, \text{ diagonal, all} \\ \text{diagonal elements are} \\ 2\underline{A}^T(\underline{\gamma}) \Lambda_o^{-1} \underline{A}(\underline{\gamma}) \end{array} \end{array} \right]^{-1} \quad \text{incoherent} \quad (\text{B-21})$$

or

$$\Lambda^{-1} = \left[\begin{array}{c|c} \begin{array}{l} 2 \times 2 \\ \text{i-j element is} \\ 2N \frac{\partial \underline{A}^T(\underline{\gamma})}{\partial \gamma_i} \Lambda_o^{-1} \frac{\partial \underline{A}(\underline{\gamma})}{\partial \gamma_j} \end{array} & \begin{array}{l} 2 \times 1 \\ \bigcirc \end{array} \\ \hline \begin{array}{l} 1 \times 2 \\ \bigcirc \end{array} & \begin{array}{l} 1 \times 1 \\ \text{element is} \\ 2N\underline{A}^T(\underline{\gamma}) \Lambda_o^{-1} \underline{A}(\underline{\gamma}) \end{array} \end{array} \right]^{-1} \quad \text{coherent} \quad (\text{B-22})$$

We see that the upper left-hand submatrix of Λ , which we will denote by Λ_1 and which contains the terms corresponding to the variances of the A and Θ estimates, is the same in the coherent and incoherent cases. To obtain the bound on the variance of any unbiased angle estimate $\hat{\Theta}$, we must evaluate the 2-2 term of Λ_1^{-1} . Remembering that

$$\underline{\gamma}^T = [A, \Theta] \quad (\text{B-23})$$

and introducing the constant sum beam-linear difference beam assumption

$$\underline{A}^T(\underline{\gamma}) = [A\Theta, A] \quad (\text{B-24})$$

the relevant partials are

$$\frac{\partial \underline{A}^T(\underline{\gamma})}{\partial A} = [\Theta, 1]$$

$$\frac{\partial \underline{A}^T(\underline{\gamma})}{\partial \Theta} = [A, 0] \quad (\text{B-25})$$

and using

$$\Lambda_o = \begin{bmatrix} 2\sigma^2 & 0 \\ 0 & 2\sigma^2 \end{bmatrix} \quad (\text{B-26})$$

we obtain

$$\Lambda_1 = \frac{N}{\sigma^2} \begin{bmatrix} (1 + \theta^2) & A\theta \\ A\theta & A^2 \end{bmatrix} \quad (\text{B-27})$$

and

$$\Lambda_1^{-1} = \frac{\sigma^2}{N} \begin{bmatrix} 1 & -\theta/A \\ -\theta/A & \frac{(1 + \theta^2)}{A^2} \end{bmatrix} \quad (\text{B-28})$$

Thus, using Eq. (B-7), we have obtained the lower bound on angular precision as

$$\sigma_\theta \geq \left[\frac{1}{N} \frac{\sigma^2}{A^2} (1 + \theta^2) \right]^{1/2} \quad (\text{B-29})$$

and, recalling our convention that

$$\frac{E}{N_0} = \frac{A^2}{\sigma^2} \quad (\text{B-30})$$

the bound becomes

$$\sigma_\theta \geq \left[\frac{1}{N} \frac{1}{E/N_0} (1 + \theta^2) \right]^{1/2} \quad (\text{B-31})$$

matching Eq. (7) of Sec. III-C-1.

To obtain the bound in the biased case, we must evaluate the matrix Q of Eq. (B-1) using the bias data from the simulation. We begin by partitioning the Q matrix as

$$Q = \begin{bmatrix} R & S \\ U & V \end{bmatrix} \quad (\text{B-32})$$

R is 2×2 and contains the partials of \underline{m} with respect to A and θ (α_1 and α_2). In the incoherent case, V is $N \times N$, S is $2 \times N$, and U is $N \times 2$. In terms of these submatrices, the upper left-hand 2×2 submatrix of the bounding matrix $Q^T \Lambda^{-1} Q$ is

$$C^\gamma = R^T \Lambda_1^{-1} R + U^T \Lambda_2^{-1} U \quad (\text{B-33a})$$

where

$$\Lambda = \begin{bmatrix} \Lambda_1 & & 0 \\ 2 \times 2 & & \\ & & N \times N \\ 0 & & \Lambda_2 \end{bmatrix} \quad (\text{B-33b})$$

We are specifically interested in the 2-2 term of C^γ , which is the bounding variance of $\hat{\theta}$. The contribution to this term by the product $U^T \Lambda_2^{-1} U$ is

$$C_{22}^{\gamma} = L \sum_{k=1}^N U_{k2}^2 \quad (\text{B-34})$$

where L is the common diagonal term of Λ_2^{-1} , and the summation is the sum of the squares of the elements of the second column of U . The second column of U contains the elements U_{k2} which, using Eq. (B-2), are

$$U_{k2} = \frac{\partial m_2}{\partial \psi_k} = \frac{\partial E(\hat{\Theta})}{\partial \psi_k} \quad (\text{B-35})$$

Because the complex noise samples in each channel are distributed with circular symmetry, the statistical properties of any estimator $\hat{\Theta}$ will be independent of the ψ_i . Thus, the U_{k2} are zero, and there is no contribution to the bounding variance of $\hat{\Theta}$ by the term $U^T \Lambda_2^{-1} U$.

The problem is then reduced to determining the elements of R . The 2-2 term of $R^T \Lambda_1^{-1} R$ is

$$C_{22}^{\gamma} = R_{12}^2 \lambda_{11} + R_{22}^2 \lambda_{22} + 2R_{12} R_{22} \lambda_{12} \quad (\text{B-36})$$

where the λ s are the elements of Λ_1^{-1} , and we have used the fact that Λ_1 is real and symmetric. Thus, the elements needed are R_{12} and R_{22} , i. e.,

$$\begin{aligned} R_{12} &= \frac{\partial m_2}{\partial \gamma_1} = \frac{\partial E(\hat{\Theta})}{\partial A} \\ R_{22} &= \frac{\partial m_2}{\partial \gamma_2} = \frac{\partial E(\hat{\Theta})}{\partial \Theta} \end{aligned} \quad (\text{B-37})$$

These partials were evaluated at various values of A , Θ , and N by making small perturbations in A and Θ , running the simulation of the approximate incoherent estimator, and taking ratios of finite differences. The matrix Λ_1^{-1} has already been determined in Eq. (B-28). By combining R and Λ_1^{-1} in accordance with Eq. (B-36), the bounds of Figs. 17(a) through (c) were obtained.

ACKNOWLEDGMENT

The author is indebted to Dr. Edward M. Hofstetter for calling attention to the analysis on which the simulation is based, for numerous discussions during the course of the work, and for reviewing the manuscript upon its completion.

REFERENCES

1. E. M. Hofstetter, "The Theory of Amplitude Comparison Monopulse Radar in a Cluttered Environment," Proceedings of XIX Meeting of Avionics Panel of AGARD, Istanbul, Turkey, 25-29 May 1970.
2. H. Cramér, Mathematical Methods of Statistics (Princeton Press, Princeton, New Jersey, 1946).
3. E. M. Hofstetter, private communication.

| DOCUMENT CONTROL DATA - R&D | | |
|---|---|-----------------|
| <i>(Security classification of title, body of abstract and indexing annotation must be entered when the overall report is classified)</i> | | |
| 1. ORIGINATING ACTIVITY (Corporate author) | 2a. REPORT SECURITY CLASSIFICATION | |
| Lincoln Laboratory, M.I.T. | Unclassified | |
| | 2b. GROUP | |
| | None | |
| 3. REPORT TITLE | | |
| Multiple-Pulse Monopulse Accuracy | | |
| 4. DESCRIPTIVE NOTES (Type of report and inclusive dates) | | |
| Technical Report | | |
| 5. AUTHOR(S) (Last name, first name, initial) | | |
| Pruslin, Dennis H. | | |
| 6. REPORT DATE | 7a. TOTAL NO. OF PAGES | 7b. NO. OF REFS |
| 19 November 1971 | 40 | 3 |
| 8a. CONTRACT OR GRANT NO. F19628-70-C-0230 | 9a. ORIGINATOR'S REPORT NUMBER(S) | |
| b. PROJECT NO. 627A | Technical Report 487 | |
| c. | 9b. OTHER REPORT NO(S) (Any other numbers that may be assigned this report) | |
| d. | ESD-TR-71-302 | |
| 10. AVAILABILITY/LIMITATION NOTICES | | |
| Approved for public release; distribution unlimited. | | |
| 11. SUPPLEMENTARY NOTES | 12. SPONSORING MILITARY ACTIVITY | |
| None | Air Force Systems Command, USAF | |
| 13. ABSTRACT | | |
| <p>This report presents results from a simulation of an amplitude comparison monopulse system employing pulse integration (multiple pulses). Maximum-likelihood-angle estimators and approximations to them are derived. The accuracies (precision and bias) of these estimators are obtained by computer simulation for coherent and incoherent processing, and targets located on- and off-boresight. Results are presented as functions of signal-to-noise ratio and number of pulses integrated. The effects of imperfect knowledge of target doppler, phase, and amplitude are included. Theoretical bounds on the precision of the estimators are derived and compared with the simulation results.</p> | | |
| 14. KEY WORDS | | |
| monopulse systems pulse integration | angle estimators computer simulation | angle accuracy |